

ULRR

Simulation of droplet size distribution of emulsions produced continuously using a vortex-based cavitation device: An ensemble approach based on CFD, PBM and ANN models

Item Type	Article
Authors	Gode, Amol;Ranade, Vivek
Citation	Chemical Engineering Research and Design 224 PP. 319-333
DOI	10.1016/j.cherd.2025.11.010
Publisher	Elsevier
Rights	Attribution-NonCommercial-ShareAlike 4.0 International
Download date	2026-06-08 02:33:00
Item License	http://creativecommons.org/licenses/by-nc-sa/4.0/
Link to Item	https://hdl.handle.net/10344/31460



Simulation of droplet size distribution of emulsions produced continuously using a vortex-based cavitation device: An ensemble approach based on CFD, PBM and ANN models

Amol Gode , Vivek V. Ranade ^{*} 

Multiphase Reactors and Intensification Group, Bernal Institute, University of Limerick, Limerick V94T9PX, Ireland

ARTICLE INFO

Keywords:

Hydrodynamic cavitation
Collapsing cavities
Energy dissipation rate
CFD
PBM

ABSTRACT

Emulsions find applications in varied industries like food and beverage, cosmetics and pharmaceuticals. Droplet size distribution (*DSD*) determines many critical quality attributes of an emulsion. An ability to simulate *DSD* is therefore pivotal to design devices for obtaining emulsions of desired *DSD* and properties. In this work, we present an ensemble approach for modelling the *DSD* of emulsions produced continuously using a vortex-based hydrodynamic cavitation (VD) device. The developed approach and computational models are evaluated by comparing the simulated results with the experimental data. Experiments on the continuous production of rapeseed oil in water emulsions (with Tween 20 as surfactant) were carried out at different operating parameters. The turbulent, three phase (gas-liquid-liquid) cavitating flow in a vortex-based cavitation device was simulated using the Eulerian approach. A population balance model with appropriate breakage kernels was developed and included with the computational fluid dynamics (CFD) model. The measured *DSD* was found to be bimodal, indicating two different breakage mechanisms (one based on turbulent shear and the other based on collapsing cavities). A novel methodology was developed to account for highly localised intense energy dissipation rates generated by collapsing cavities for simulating *DSDs*. The localised intense energy dissipation rates due to cavities were estimated using a previously developed artificial neural network (ANN). The predictions of *DSD* obtained with the developed methodology based on CFD, PBM and ANN showed good agreement with the experimental data. The presented approach and results will be useful for designing vortex-based cavitation devices for producing emulsions. The work will also provide a useful basis for developing multi-scale computational models for simulating the *DSD* of emulsions generated by hydrodynamic cavitation devices.

1. Introduction

Emulsions, where fine drops of an immiscible liquid are dispersed in a continuous phase, play crucial roles across various industries, including food processing, pharmaceuticals, cosmetics, and chemical (Thaker and Ranade, 2023a). The different equipment used for producing emulsions can be operated in either a batch or continuous mode. The continuous mode of operation offers several advantages in terms of reliable product quality, quick response to market demands or changes in product formulation and reduced costs (O'Sullivan et al., 2015; Håkansson, 2018). In this work, we focus on the continuous mode of generating emulsions.

Various devices, such as colloid mills, rotor-stators, high-pressure homogenizers, ultrasonicator, and membranes, have been used for

generating emulsions (Perrier-Cornet et al., 2005). In recent years, hydrodynamic cavitation (HC) based emulsification devices are being increasingly used and have shown to produce stable emulsions with finer droplet sizes and at lower energy consumption (Carpenter et al., 2022, 2017; Panda et al., 2020). HC is a process that involves the formation and collapse of vapour bubbles in a liquid flow. The collapsing bubbles or cavities generate intense shear forces, very high localised energy dissipation rates and shock waves (Pandit et al., 2021). Encounter of droplets of dispersed phase with these collapsing cavities leads to droplet breakage and thereby producing fine emulsion at lower energy consumption (Zhang et al., 2016). Recent works on hydrodynamic cavitation for emulsification include the use of devices like orifices (Carpenter et al., 2017; Ramisetty et al., 2014; Schlender et al., 2015), liquid whistle orifice (Parthasarathy et al., 2013), circular and slit venturi (Carpenter et al., 2017; Patil and Gogate, 2018), valve type

* Corresponding author.

E-mail address: vivek.ranade@ul.ie (V.V. Ranade).

<https://doi.org/10.1016/j.cherd.2025.11.010>

Received 21 June 2025; Received in revised form 9 November 2025; Accepted 11 November 2025

Available online 14 November 2025

0263-8762/© 2025 The Author(s). Published by Elsevier Ltd on behalf of Institution of Chemical Engineers. This is an open access article under the CC BY license (<http://creativecommons.org/licenses/by/4.0/>).

Nomenclature		V_T	throat velocity, m/s
Q_D	Volumetric flow rate through the emulsification device, m^3/s	V_D	Volume of the emulsification device, m^3
Q_C	Volumetric flow rate in the circulation loop, m^3/s	<i>Greek Letters</i>	
q_{net}	net volumetric flow rate, m^3/s	α	volume fraction, -
$g(V)$	breakage frequency, 1/s	ρ	density, kg/m^3
C_2, C_3, C_4	model parameters in Alopaeus et al. breakage model	μ	viscosity, $kg/m\ s$
d	droplet diameter, μm	σ	interfacial tension, N/m
γ_i	bin fraction, -	η	energy efficiency for droplet breakage, %
v_i	velocity of mixture in cell i , m/s	$\bar{\epsilon}$	average energy dissipation rate per unit mass in the device, m^2/s^3
A_i	area of cell i , m^2	<i>Subscript</i>	
Δx_i	width of bin or diameter group	O	organic phase
ϵ_{cav}	turbulent energy dissipation rate due to cavitation, m^2/s^3	A	aqueous phase
α_{vc}	critical vapour fraction, -	m	mixture phase
α_{vu}	upper limit of vapour fraction, -	<i>Acronyms</i>	
P_{cz}	average pressure in the effective cavitation zone, Pa	CFD	Computational fluid dynamics
P_{cz}^a	amplitude of pressure fluctuations, Pa	DSD	Drop size distribution
f_{cz}	frequency of pressure fluctuations, kHz	VD	Vortex-based hydrodynamic cavitation device
$\bar{\epsilon}$	mean energy dissipation rate, m^2/s^3	HC	Hydrodynamic cavitation
R_0	initial cavity radius, μm	PBM	Population Balance Model
d_{32}	Sauter mean diameter, μm	ANN	Artificial Neural Network
d_T	throat diameter, mm	PDF	Probability density function
ΔP	inlet pressure drop, kPa	RO	Rapeseed oil
Q	volumetric flow rate, m^3/s	DI	Deionized
t	time, s		

(Pang and Ngaile, 2021), vortex-based devices (Gode et al., 2024), swirling jet devices (Gode et al., 2024), swirling cavitation chamber device (Yang et al., 2018) and so on.

Vortex-based hydrodynamic cavitation devices (VD) exhibit early inception of cavitation and maintain a cavitating core that shields the device from erosion - leading to consistent performance over a long time (Sarvothaman et al., 2024; Thaker and Ranade, 2022; Gode et al., 2023). In such a device, a strong swirling flow is established in the vortex chamber of the device, which leads to low pressure zone and the generation of cavities. When these cavities experience turbulent pressure fluctuations and travel downstream, they collapse and realise highly localised intense shear and energy dissipation rates. The interaction of oil droplets with highly localised, very high energy dissipation rates generates fine droplets. Recently, our group has demonstrated that VD are quite effective in producing liquid-liquid emulsions (Thaker and Ranade, 2023a; Upadhyay et al., 2024). HC and in particular, VD has a significant potential for producing emulsions at low operating pressure drops and costs. The cavitation device used in this work has been used for emulsification of various oil and aqueous phase systems (for example, dense emulsions of rapeseed oil-in-water (Upadhyay et al., 2024), coconut oil-in-water by Upadhyay and Ranade (Upadhyay and Ranade, 2025)) as well as for high viscosity single phase flows (Thaker et al., 2023) and thick biomass slurries (Islam and Ranade, 2025). In this work, we have used VD for continuously generating rapeseed oil-in-water emulsions and characterised droplet size distributions (DSDs) of generated emulsions.

DSD is one of the key attributes defining the quality of emulsions (Maindarkar et al., 2015; Lebaz et al., 2022) and therefore significant research efforts have been devoted to developing models capable of simulating the DSD of emulsions. Population balance models (PBM) coupled with computational fluid dynamics (CFD) models are widely used to simulate the DSD of emulsions (Maindarkar et al., 2015; Lebaz et al., 2022; Janssen and Mayer, 2016; Calvo et al., 2024; Michael et al., 2017; Raikar et al., 2009; Dubbelboer et al., 2014). These models account for the dynamics of droplet breakage and if relevant, coalescence during emulsification processes. Most of the literature about the use of

the CFD+PBM approach for estimating DSD of emulsions is directed towards emulsification in devices like high-pressure homogenizers (Becker et al., 2014) and rotor-stator type (Michael et al., 2017; Qin et al., 2016) operated in a batch mode. The prediction of DSD of emulsions produced in a continuous mode without loop configuration using static mixers has been reported by Lebaz et al. (2022). In our group, earlier attempts to use coupled CFD and PBM models for simulating drop breakage by hydrodynamic cavitation did not account for breakage caused by collapsing cavities and therefore were not able to simulate the generation of finer droplets observed in the experiments (Thaker and Ranade, 2023a). Recently, Pandey and Ranade (Pandey et al., 2024) have presented simplified models for simulating droplet breakage caused by collapsing cavities generated in VD. However, coupled CFD and PBM model accounting for droplet breakage by collapsing cavities in a continuous mode of operation is not yet available. In this work, we have bridged this gap.

We present a novel methodology and an ensemble CFD+PBM+ANN approach for simulating the continuous production of emulsions. The methodology was applied for simulating drop breakage and the emulsification process using VD. For validation of the proposed methodology, the required experimental data was obtained by operating the VD in a loop at varying operating conditions of pressure drop and emulsion flow rates. An integral component of this new approach is the development of CFD methodology for simulating flow in a continuous loop-based set-up. For simulating droplet breakage using PBM, the basic framework developed by Alopaeus et al (Alopaeus et al., 2002). was used. The proposed novel approach captures the experimentally observed bimodal droplet size distribution by combining the CFD+PBM model with the previously developed ANN model (Ranade and Ranade, 2023) and incorporating localised intense dissipation zones generated by collapsing cavities in the breakage rate formulation. The presented data, approach and models will be useful for simulating the production of emulsions using VD in a continuous mode. The validated models will pave the way towards realising optimum design and operating parameters for producing emulsions of desired DSD on an industrially relevant scale. The approach is generic and can be used for simulating emulsions

generated using other HC devices.

2. Experimental

An experimental set-up for producing oil in water emulsions in a continuous mode was designed and established. The schematic of the experimental set-up is shown in Fig. 1. A photograph of the experimental set-up is shown in Figure S1 of the supplementary information.

The experimental set-up consisted of two feed tanks containing DI water (with surfactant) and rapeseed oil. The flow rates of the two feed streams were regulated by means of two separate peristaltic pumps (Longer Intelligent Peristaltic Pump L300–1F) calibrated for water and rapeseed oil, respectively. A T-junction connector was used to connect the two inlet streams to the loop circuit. A peristaltic pump (Masterflex Easyload pump with single head) was used to circulate the mixture of emulsion and incoming feed streams in the loop arrangement. A gas disengagement section was included in the experimental setup after the emulsification device to allow for trapped gases to be removed from the flow stream. An external circulation loop with the emulsification device was used to increase the residence time and increase the probability of oil droplets encountering the cavitation zone in the device. The mean energy dissipation rate per unit mass in the emulsification device is given by:

$$\bar{\epsilon} = \frac{\Delta P Q}{\rho_m V_D} \quad (1)$$

where ΔP is the pressure drop across the emulsification device, Q is the flow rate through the device, ρ_m is the mixture density and V_D is the volume of the emulsification device. The circulation loop flow rate was varied to change the mean energy dissipation of the emulsification device. The digital pressure gauge (Digitron 2000 P) and a flow meter (Krohne Magnetic Flowmeter – AF-E 400) were placed before and after the emulsification device, respectively, for measuring the pressure drop and flow rate through the vortex-based HC device (Gode et al., 2024).

The experiments were performed using a vortex-based hydrodynamic cavitation device, VD (based on the design of Vivira Process Technologies and the patent of Ranade et al (Vivek Ranade and Bhandari, 2013)). VD with a nominal capacity of 1 LPM (throat diameter, $d_T = 3$ mm) was used in the present work. The detailed dimensions of the VD used in this work, with reference to the throat diameter, were the same as reported by Simpson and Ranade (Simpson and Ranade, 2019a). The oil-in-water emulsion were produced using rapeseed oil ($\rho_o = 915$ kg/m³, $\mu_o = 6.2 \times 10^{-2}$ Pa.s, sourced from Newgrange Gold, Tesco, Ireland) and deionised (DI) water ($\rho_A = 1000$ kg/m³, $\mu_A = 0.001$ Pa.s, sourced from Elga ultrapure water system). Tween 20 (sourced from MP Biomedicals, LLC, France) was used as a surfactant to stabilise the emulsion. Based on previous studies (Gode et al., 2024), 2 wt% of Tween 20 was used for all experiments. The interfacial tension of the rapeseed

oil/water system was obtained from literature as 0.035 N/m (Thaker and Ranade, 2023a; Nakamoto et al., 2017). The net emulsion flow rate out from the device and pressure drop across the device were varied to obtain emulsions with varying characteristic diameters. Since the focus of this work is on developing an approach and model for simulating *DSD* of emulsions generated continuously using VD, experiments were restricted to only one volume fraction of oil (0.05). It was shown in one of our earlier studies that *DSD* does not depend on oil volume fraction up to 35 % (Upadhyay et al., 2024). The operating parameters used for carrying out experiments are listed in Table 1.

The emulsion samples were collected from the outlet port after establishing that steady state is achieved. The steady state was ascertained by performing specific experiments and collecting samples at every residence time (ratio of overall system volume and net flow rate of emulsion). It was established that the change in *DSD* is marginal after three residence times, and the change in the Sauter mean diameter beyond three residence times was less than 2 %. The experimental data reported in this work was based on samples collected after at least five residence times. The experimental data verifying the steady state are included in Section S3 of the supplementary information. The collected samples were analysed using Malvern MasterSizer 3000. The refractive index for rapeseed oil was set to 1.466 for the lasers [red laser (632.8 nm) and blue laser (470 nm)]. Water was used as a dispersant medium (water) at room temperature (20 °C). The experiments were performed three times to quantify error bars. The error bars on measured *DSD* and Sauter mean diameter values are included wherever possible.

3. Computational model

The droplet breakage in a vortex-based HC device is predominantly a result of cavitating flow generated due to a strong swirl established in the vortex chamber. The flow characteristics and cavitation inception in VD were numerically investigated by Thaker et al. (2023) using the Eulerian mixture model approach for simulating gas-liquid flow at varying viscosity values, and the simulation results showed good agreement with experimental values of pressure drop and cavitation inception. The collapse of cavities generated due to swirling flow results in localised intense shear and energy dissipation rates, leading to fine emulsions. Thaker and Ranade (2023a) attempted to simulate the *DSD* of emulsions produced using VD operated in a batch mode using the PBM

Table 1
Operating parameters of the continuous experiments.

Parameter	Values / Range
Pressure drop (ΔP), kPa	150, 200, 250
Flow rate ratio (Q_D/q_{net}), -	5, 10, 50
Flow rate through device (Q_D), LPM	1.0, 1.2, 1.35
Oil volume fraction (α_{oil}), -	0.05

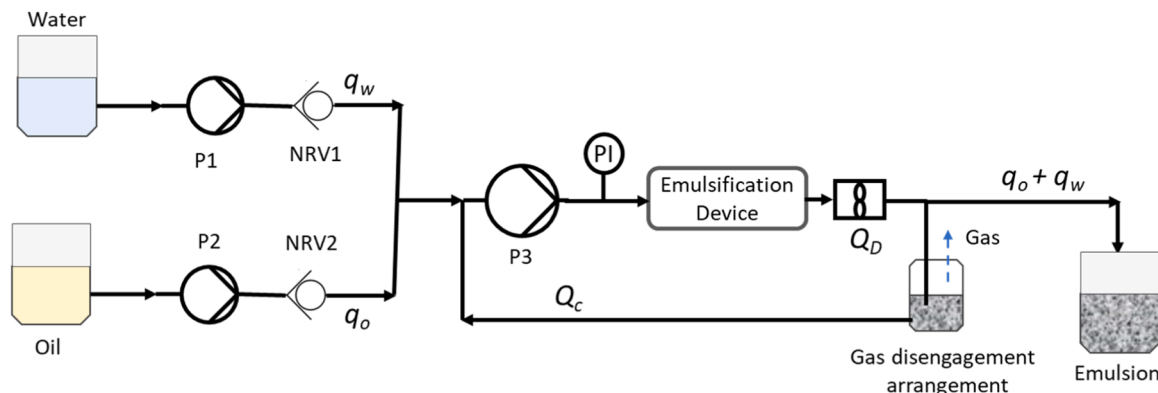


Fig. 1. Schematic of experimental setup used for continuous emulsion production.

approach. However, their model was not able to simulate fine droplets generated by VD primarily because of a lack of appropriate accounting of breakage caused by localised intense energy dissipation zones created by collapsing cavities.

In this work, we developed a novel approach to simulate droplet breakage caused by collapsing cavities generated in VD. The details of the CFD+PBM model equations and solution methodology used in the present work is same as that of Thaker and Ranade (2023a) and for the sake of brevity, these details are discussed in brief here. Specific details of CFD+PBM model used in the present work along with the breakage kernels are discussed in Section 3.1. The novel approach and modifications to the breakage kernel for accounting the influence of highly localised intense energy dissipation rates caused by collapsing cavities are discussed in Section 3.2. The approach for simulating continuous production of emulsions using VD operated in a loop configuration is presented in Section 3.3. The modified domain and boundary conditions needed for this are discussed. In Section 3.4, an overview of the ensemble approach incorporating CFD, ANN and PBM models is presented.

3.1. CFD-PBM model for DSD prediction

The application of various multiphase modelling approaches like Eulerian–Eulerian, Eulerian – Lagrangian as well as Eulerian – Lagrangian – VOF models for simulating cavitating flows in vortex devices is available (Simpson and Ranade, 2019a; Wang et al., 2025; Li et al., 2023). Each of these approaches have distinct pros and cons (discussed in books by Ranade (Ranade and Utikar, 2022; Ranade, 2002)). In this work, the focus is on understanding cavitation induced droplet breakage. The breakage induced by collapsing cavities occurs mainly outside of the vortex core and therefore the Eulerian approach was considered adequate. This choice was also supported by previous studies of simulations of emulsions in vortex based (Thaker and Ranade, 2022, 2023a, 2023b) and other devices (Fathi Roudsari et al., 2012; Sun et al., 2021; Liu and Yu, 2025). Following Thaker and Ranade (2023a), the numerical approach adopted in this study uses the mixture multiphase model for simulating cavitating flow and PBM for modelling droplet breakage and evolution of DSD in the continuous emulsification setup. The multiphase flow was considered to include three phases, i.e., water (primary), water vapour (secondary phase through cavitation) and oil (secondary). The material properties stated in Section 2 were used to define the density and viscosity values of the different phases in the simulation model. Following the experimental conditions, the volume fraction of secondary phase oil was set to 0.05.

The selection of turbulence model is based on some earlier studies which employed various turbulence models including two-equation models (Simpson and Ranade, 2019a, 2019a, 2019b), Reynolds stress models (Simpson and Ranade, 2019a) and LES models (Pandare and Ranade, 2015; Shamami and Birouk, 2008; Hoekstra et al., 1999) for simulating flow in VD. A detailed analysis of these previous studies indicated that the unsteady RANS SST $k-\omega$ turbulence model captures adequate details of the cavitating flows such as inception pressure drop, pressure drop versus flow relationship as well as radial profiles of tangential velocity very well without excessive demands on computing resources (Gode et al., 2023; Thaker et al., 2023; Simpson and Ranade, 2019a). The results with SST $k-\omega$ turbulence model were comparable to the more resource-intensive RSM (Simpson and Ranade, 2019a; Pandare and Ranade, 2015) and LES (as discussed in (Pandare and Ranade, 2015)). There are several other published studies which support the choice of SST $k-\omega$ model for simulating turbulence swirling flows (see for example, (Michael et al., 2017; Sun et al., 2021; Nie et al., 2024; Chen et al., 2024; Bagkeris et al., 2019)). Based on these considerations and prior studies, the URANS SST $k-\omega$ model was used in the present work.

The cavitating flow in VD was simulated by the model proposed by Singhal et al. (2002) which is based on the Rayleigh-Plesset equation for vapor bubble dynamics, accounting for non-condensable gases. Its

suitability and validation for use within this specific vortex-based cavitation device has been previously established in the work by (Simpson and Ranade, 2019a; Thaker and Ranade, 2023a). There are several other studies using the Singhal cavitation model for similar flows (see for example, (Athavale et al., 2002; Ye et al., 2022)). The effect of non-condensable gas or air ($\rho = 1.225 \text{ kg/m}^3$ and $\mu = 1.78 \times 10^{-5} \text{ kg/m.s}$) was included in the cavitation model with the mass fraction of non-condensable gas fixed at 15 ppm as suggested in the works of Singhal et al. (2002). Additional details on the equations of the CFD model used here are provided in supplementary information Section S1.

The drop breakage and drop size distribution evolution in the domain is simulated using the population balance model (PBM). The PBM methodology adopted was similar to that discussed by Thaker and Ranade (2023a). In an earlier work, Thaker and Ranade (2023b) studied the influence of surfactant concentration on the DSD of emulsions produced using a vortex-based hydrodynamic cavitation device and varied the surfactant concentration from 1 % to 8 %. Their results indicated that with a surfactant concentration of 2 %, the emulsion was stable for at least 74 days without significant change in the DSD at quiescent conditions. Under the dynamic conditions, it is important to consider following key characteristic time scales while understanding influence of coalescence on evolution of DSD: surfactant adsorption time scale, droplet contact time scale during collisions and film drainage or coalescence time scales. Surfactant molecules adsorb on droplet surface and prevent coalescence. When a droplet breaks, new surface area is generated. In such cases, it is important to consider and compare adsorption time scales and coalescence time scales. If adsorption time scales are much smaller than coalescence time scales, coalescence need not be considered since surfactant molecules will quickly cover newly created surface and prevent coalescence. Coalescence occurs when droplets collide, are in contact with each other and the film between these droplets drains. If the droplet contact time is much smaller than the film drainage time, coalescence will not occur and therefore coalescence need not be considered in the PBM. In absence of data on dynamic interfacial tension which is needed for estimating adsorption time scales, the droplets contact, and film drainage time scales were examined. For the VD considered in this work, mean energy dissipation rates in the device (ϵ) are in the range of 10^2 – $10^4 \text{ m}^2/\text{s}^3$. The characteristic collision or contact times (τ_c) estimated as $\tau_c \sim d^{2/3}/\epsilon^{1/3}$ (Ni (2024)) for droplet diameters (d) in the 1–100 μm range were found to be extremely short, in the range of microseconds to sub-millisecond. By contrast, film-drainage or coalescence times for oil droplets in the presence of Tween-20 are typically measured or estimated in the range of 0.1–30 s (Bachnak et al., 2024; Kamp et al., 2017; Politova et al., 2017). The contact time in the intense hydrodynamic environment of the vortex device is therefore significantly smaller than the drainage time, rendering coalescence kinetically improbable. Considering this and the concentrations of surfactant used (2 % w/v Tween 20, well above the critical micelle concentration), coalescence was not included in the PBM (Thaker and Ranade, 2023a; Lebaz et al., 2022; Maaß and Kraume, 2012).

The PBM requires specification of appropriate functions for describing the breakage processes. Binary breakage is assumed following the general practice. The binary breakage assumption avoids complexity arising from considering multiple daughter droplets from parent droplets, which can also be considered as a series of binary breakage events (Håkansson, 2020). In this work, we used the breakage model of Alopaeus et al. (2002) (later modified by Laakkonen et al. (2006)) for the liquid-liquid emulsion as this model uses the dispersed phase viscosity (μ_o) in the breakage frequency kernel, consistent with the mechanism of droplet deformation and breakup. The breakage frequency of droplets of volume V to smaller droplets is given by:

$$g(V) = C_2 \epsilon^{1/3} \operatorname{erfc} \left(\sqrt{\frac{C_3 \sigma}{\rho_A \epsilon^{2/3} d^{5/3}} + \frac{C_4 \mu_o}{\sqrt{\rho_A \rho_o} \epsilon^{1/3} d^{4/3}}} \right) \quad (2)$$

Where C_2 , C_3 and C_4 are model parameters, d is the droplet diameter, ρ_A is the density of the aqueous phase, μ_O is the viscosity of the oil phase, σ is the surface tension and ε is the energy dissipation rate. This equation represents terms corresponding to drop breakage due to eddy-drop interaction and includes both surface and viscous forces. The term containing the parameter C_2 represents the frequency of droplet breakage and influences the broadness of the *DSD* without significantly impacting the location of the peak. The parameter C_3 is related to the breakage probability and influences the location of the peak as well as the broadness of the *DSD*. The values of the parameter appearing in Eq. (2) were used from the previous work of Thaker and Ranade (2023a) since the model was able to capture larger droplets generated via turbulent shear. It can be seen from Eq. (2) that the breakage frequency depends on the product of C_3 and σ and therefore the product ($C_3\sigma$) can be treated as one parameter. As long as the value of ($C_3\sigma$) is the same, simulated *DSD* will be the same (see Figure S6 of the supplementary information). In this work, we have used the same oil, water and surfactant system as used in (Thaker and Ranade, 2023a) and therefore the parameters C_2 , ($C_3\sigma$) and C_4 as reported, were used in the present work. Considering the treatment of ($C_3\sigma$) as one parameter, accurate measurement of interfacial tension in the presence of surfactants was not needed.

The CFD+PBM model presented by Thaker and Ranade (2023a) does not explicitly account for breakage due to collapsing cavities and therefore was unable to capture fine droplets generated via collapsing cavities. They suggested the inclusion of two different ranges of turbulent energy dissipation rate values: one that is generated via convective flow in the VD chamber and the other that is generated via collapsing cavities. Incorporation of such two levels of energy dissipation rates could lead to the prediction of bi-modal *DSD* observed in experiments. The present approach was developed by (a) including the influence of collapsing cavities by incorporating localised high energy dissipation rates in the PBM breakage model (Section 3.2) and (b) modifying the model to extend the applicability to continuous emulsion production (Section 3.3).

3.2. Representing localised energy dissipation rates generated by collapsing cavities

The fine droplets are generated in a hydrodynamic cavitation device because of the intense localised energy dissipation zones generated by collapsing cavities. The extent of breakage caused by cavitation in any specific HC device therefore depends on (a) the zone in which collapsing cavities are present and (b) the intensity of collapse, which determines the value of localised energy dissipation rate. The device scale CFD models can be used to identify the region in which cavitation occurs (see, for example, the works of (Thaker and Ranade, 2023a; Gode et al., 2023; Simpson and Ranade, 2019a; Ranade, 2022)). The device-scale CFD model, however, is not capable of estimating the intensity of cavity collapse. Typically, the intensity of collapse is estimated by simulating micro-scale dynamics of a single or a group of cavities (for example (Pandit et al., 2021; Pawar et al., 2017)). Machine-learning based surrogate models have also been developed, which mimic the results of the full cavity dynamics model (Ranade and Ranade, 2023). In this work, we developed a novel methodology to combine a device-scale CFD model with a machine learning based cavity dynamics model to estimate the cavitation zone and energy dissipation rates generated by collapsing cavities. This approach, together with PBM, was applied to simulate drop breakage in a vortex-based HC device.

The CFD model provides the distribution of vapour volume fraction within the device. The region having a non-zero vapour fraction may be termed as a cavitating region. Cavities are generated in this region, experience pressure fluctuations as they travel (typical lifetime of cavities is less than 1 ms) and collapse, which leads to localised high energy dissipation rates. Not all the cavitation region is effective for droplet

breakage. There will be upper and lower limits of vapour volume fraction within which effective droplet breakage may occur. If the vapour volume fraction is beyond a certain value (α_{vu}), cavities may be very close to each other and may not collapse. If the vapour fraction is lower than a certain value (α_{vc}), the probability of encounter between a collapsing cavity and a droplet becomes small, and breakage may not occur. A sample of the simulated distribution of vapour volume fraction is shown in Fig. 2.

The cavitating region in the vortex-based device was identified based on the region with non-zero vapour fraction. The cavities are generated in the vortex core. These cavities collapse as they travel to high pressure region and experience pressure fluctuations. The time scales of cavity collapse are very small ($\sim 10^{-4}$ s) and therefore the distance travelled by cavities is quite small ($\sim 10^{-3}$ m). In the vortex core, where the gas volume fraction is close to unity, cavity collapse does not occur. In Eulerian multiphase flow simulations, the limiting vapour fraction value for distinguishing the gas and liquid interface typically falls between 0.5 and 0.66 (Ranade, 2002, 2022). Following this, in this study, the upper limit of vapour fraction (α_{vu}) was set at 0.6. This means that if the volume fraction is more than 0.6, cavity collapse will not occur, which is a reasonable approximation considering the physics of cavity collapse. As the vapour volume fraction decreases, there is a lower chance of an encounter between the collapsing cavity and the droplet. For representing this, it was decided to use a lower limit of volume fraction (α_{vc}) for identifying the effective region for droplet breakage induced by cavity collapse. The value of the lower limit (α_{vc}) was determined through a sensitivity study (discussed in Section 4.2) and comparison with experimental *DSD*.

The localised intense energy dissipation value due to cavity collapse (ε_{cav}) can be applied in the effective cavitation region identified by α_{vc} . The value of ε_{cav} depends on five parameters, namely initial cavity radius, ambient pressure and temperature, and frequency and amplitude of pressure fluctuations (Pandit et al., 2021; Ranade and Ranade, 2023). For the hydrodynamic cavitation devices, the values of ε_{cav} were found to be in the range of 10^7 - 10^9 m²/s³ (Thaker and Ranade, 2023a). In this work, instead of solving full cavity dynamics, we have used the previously developed ANN-based surrogate model of cavity dynamics (Ranade and Ranade, 2023) for estimating the value of ε_{cav} . For obtaining the input parameters required for the ANN model, the first step was to identify the cavitation zone using the simulated flow field by the CFD model. The region of the HC device having a vapour volume fraction between α_{vc} and 0.6 was defined as an effective cavitation region. For identifying this zone, iso-volumes of vapour volume fraction equal to 0.6 and α_{vc} were generated. Once the cavitation zone was identified, the volume-averaged values of pressure (P_{cz}), turbulence kinetic energy (k_{cz}) and specific dissipation rate (ω_{cz}) in the cavitation zone were obtained as:

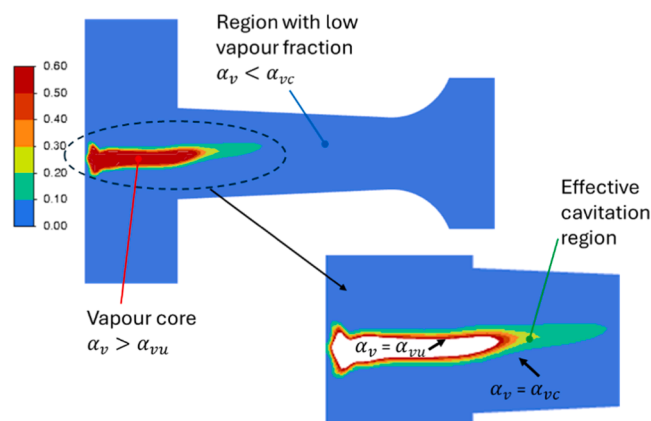


Fig. 2. Effective cavitation region for specifying localised intense energy dissipation rate.

$$P_{cz} = \frac{\int_{cz} P dv}{\int_{cz} dv}, \quad k_{cz} = \frac{\int_{cz} k dv}{\int_{cz} dv}, \quad \omega_{cz} = \frac{\int_{cz} \omega dv}{\int_{cz} dv} \quad (3)$$

The volume-averaged turbulent kinetic energy over the cavitation zone can be used for estimating the amplitude of pressure fluctuations (P_{cz}^a). Using simple dimensional arguments, one may write (Ansys® Academic Research Mechanical and CFD, 2020; Sarvothaman et al., 2019):

$$P_{cz}^a = \varnothing \rho k \quad (4)$$

Where \varnothing is a proportionality factor. In this work, we have used \varnothing as unity (Pawar et al., 2017; Moholkar and Pandit, 2001). The volume-averaged specific dissipation rate (ω_{cz}) over the cavitation zone was used for estimating the frequency of pressure fluctuations in the cavitation zone (f_{cz}) as:

$$f_{cz} = \frac{\omega_{cz}}{2\pi} \quad (5)$$

The ambient temperature was set to the temperature at which experiments were conducted (300 K). These local values of mean pressure, amplitude and frequency of pressure fluctuations and vapor fraction in the cavitation zone obtained from the CFD simulation were used in the ANN-based surrogate model to predict ε_{cav} . In order to estimate ε_{cav} , we need one more quantity, the initial cavity radius, R_0 , in addition to the operating temperature and the three parameters obtained from the device-scale CFD models (P_{cz} , P_{cz}^a and f_{cz}). The initial radius of the cavity depends on a variety of parameters like the extent and nature of dissolved gases, the presence of impurities or small dust particles, and so on (Ranade, 2022; Ranade et al., 2022). The prediction of initial cavity radius values for hydrodynamic cavitation is further complicated due to the small time and length scales of cavitation phenomena prevalent in such devices. The initial cavity radius is reported in literature to be of the order of $10^1 \mu\text{m}$ (Pandit et al., 2021; Liu and Brenner, 1995). In the present study, considering the uncertainty in estimating the initial radius of cavity, this was treated as a model parameter. Sensitivity of the predicted results with the values of initial cavity radius (R_0) was examined (discussed in Section 4.2) and an appropriate value of R_0 selected. The ANN based surrogate model (Ranade and Ranade, 2023) was then used to estimate ε_{cav} for different operating conditions using the five parameters estimated as discussed here.

The use of ANN based surrogate model for predicting the localised high energy dissipation rates reduces the adjustable parameters required and provides a physical significance for the approach adopted instead of relying on multitude of adjustable parameters. As discussed by Ranade and Ranade (Ranade and Ranade, 2023), the ANN model was trained from a recently developed cavity dynamics model by Pandit et al. (2021) which included aspects relevant to both acoustic and hydrodynamic cavitation. The ANN architecture with three hidden layers and different number of neurons (5–4–2) was found to be most effective. The transfer function 'Tansig' was used for the hidden layers and 'Purelin' for the output layer. The training of ANN was performed using MATLAB's 'trainbr' function for Bayesian regularization. The trained ANN based surrogate model was able to predict unseen data beyond the training data range. This is further shown in a recent work by Håkansson et al. (2025). This approach directly addresses the challenge of capturing highly localized turbulent energy dissipation rate due to cavity collapse that are critical for breakage, making it relevant to local flow conditions, not just bulk equipment parameters.

The CFD+PBM model was extended to include the turbulent energy dissipation rate due to cavitation (ε_{cav}) estimated using the ANN model. The values of two parameters R_0 and α_{vc} were obtained based on a sensitivity analysis. The Alopaeus et al. model (Eq. (2)) for breakage frequency $g(V')$ was modified to include droplet breakage due to two distinct phenomena of cavitation and turbulent shear by including the ε_{cav} for modelling breakage due to cavitation in the effective cavitation region defined by α_{vc} and ε in the rest of the domain as:

For, $\alpha_v < \alpha_{vc}$

$$g(V) = C_2 \varepsilon^{1/3} \operatorname{erfc} \left(\sqrt{\frac{(C_3 \sigma)}{\rho_A \varepsilon^{2/3} d^{5/3}} + \frac{(C_4 \mu_O)}{\sqrt{\rho_A \rho_O} \varepsilon^{1/3} d^{4/3}}} \right)$$

For, $\alpha_{vc} \leq \alpha_v < 0.6$

$$g(V) = C_2 \varepsilon_{cav}^{1/3} \operatorname{erfc} \left(\sqrt{\frac{(C_3 \sigma)}{\rho_A \varepsilon_{cav}^{2/3} d^{5/3}} + \frac{(C_4 \mu_O)}{\sqrt{\rho_A \rho_O} \varepsilon_{cav}^{1/3} d^{4/3}}} \right) \quad (6)$$

The relevant experimental data on cavitation induced droplet breakage is not available for formulating breakage kernels for the cavitation induced breakage. The previous work of Thaker and Ranade (2023a) was able to simulate breakage of droplets induced by shear in cavitation devices. The breakage due to cavitation may be considered similar to the breakage by shear with the value of energy dissipation rate substantially higher than that of turbulent shear. In order to minimise model parameters, we used the same breakage kernels found useful for simulating the shear induced breakage except by using ε_{cav} in the cavitation zone (see Eq. (6)). This model, which accounts for the localised, intense turbulent energy dissipation rates induced by cavitation (ε_{cav}) was used to simulate *DSD* of emulsions produced in a continuous model (see Section 4). The CFD approach used for modelling continuous generation of emulsions is discussed in the following section (Section 3.3).

3.3. CFD model for simulating continuous mode of operation

The experimental setup for the continuous production of emulsions incorporates a circulation loop and is shown in Fig. 1. The circulation loop comprises the emulsification device, a pump for circulating flow in the loop, a gas disengagement arrangement, pressure and flow sensors and tubing and fittings for connecting the different parts. The use of a circulation loop decouples the net flow rate of emulsion, and the operating conditions needed for achieving the desired *DSD*. The ratio of flow in the circulation loop (or device) to net inlet flow rate may be considered approximately equivalent to the number of passes through VD operated in a batch mode. The inclusion of the entire circulation loop in the simulation model would introduce not only added complexity with regards to modelling the different parts of the loop but also makes the overall mesh count and therefore demands on computational resources rather excessive. In the developed approach, we avoided this by considering a small section of the circulation loop as the solution domain, as shown in Fig. 3. This approximation will represent the real-world set-up reasonably well when the extent of drop breakage in the circulation loop is negligible compared to the droplet breakage occurring in VD. The turbulent energy dissipation in the vortex device ($\sim 2 \times 10^4 \text{ m}^2/\text{s}^3$) is orders of magnitude higher than any other part of the loop ($\sim 100 \text{ m}^2/\text{s}^3$). This implies that the extent of droplet breakage occurring in VD is likely to be much higher than that occurring in the circulation loop. Recently, Pandey et al. (2024) have measured and reported that the droplet breakage in the recirculation loop and pump was less than 10 % of the overall breakage caused by the cavitation device. This lends support to the approximation used in the present work.

The curtailed section of the circulation loop in the solution domain demands representing the loop by using appropriate boundary conditions. It is in principle possible to define periodic boundary conditions at the circulation inlet and outlet – that is, whatever comes out of the solution domain from the circulation outlet re-enters the domain via the circulation inlet. However, the conventional way of defining periodic boundary conditions was not directly applicable in the present case because of the presence of multiple phases and a pump between the circulation inlet and outlet. Therefore, the suitably defined velocity inlet and outlet boundary conditions were used to mimic the circulation loop without considering the entire loop. The net flow rate (q_{net}) of emulsion produced was used to obtain the inlet velocity of the oil + water mixture

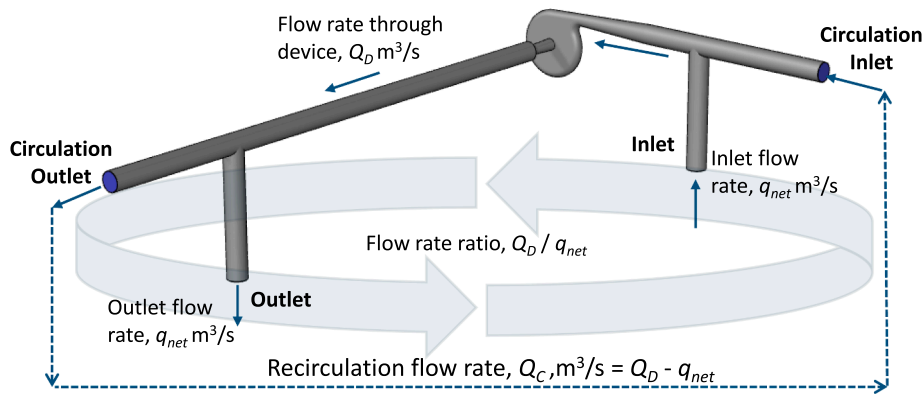


Fig. 3. Simulation domain for continuous process.

entering the domain. The volume fraction of oil (α_o) was set to 0.05 as per the experimental conditions. The flow rate (Q_D) through the device corresponding to the experimentally observed pressure drop across the device was used for specifying the boundary conditions on circulation boundaries. The flow rate ratio (Q_D/q_{net}) value was used to obtain the net emulsion flow rate (q_{net}) entering or leaving the domain.

As shown in Fig. 3, the simulation domain consisted of two inlet boundaries, one for the circulation inlet and the other for the inlet of the oil and water mixture entering the domain. Similarly, there are two outlet boundaries. For the circulation inlet and outlet, uniform velocities and volume fractions are specified as:

$$V_{inlet_circ} = -\frac{Q_D - q_{net}}{A_{in_circ}}, \alpha_{inlet_circ} = \alpha_o \quad (7)$$

$$V_{outlet_circ} = -\frac{Q_D - q_{net}}{A_{outlet_circ}}, \alpha_{outlet_circ} = \alpha_o \quad (8)$$

Where Q_D is the flow rate through the device, which is the sum of the net emulsion flow rate, q_{net} and circulation flow rate, Q_C : $Q_D = q_{net} + Q_C$. The flow rate ratio is defined by: Q_D/q_{net} . At the emulsion inlet, the following boundary conditions were used:

$$V_{inlet_qnet} = \frac{Q_D/A_{inlet_qnet}}{Q_D/q_{net}}, \alpha_{inlet_qnet} = \alpha_o \quad (9)$$

At the emulsion outlet boundary, constant pressure outlet boundary condition was used:

$$P_{outlet_qnet} = P_{ref} \quad (10)$$

Where P_{ref} is reference pressure used in the simulations. For the walls of the simulation domain, the standard no-slip boundary condition was imposed. The net flow rate of water and oil entering the domain was obtained by setting the desired flow rate ratio (for example, $Q_D/q_{net} = 10$).

The DSD at the inlet boundary for PBM simulations was obtained from the experimental data for the flow of oil and water through the circulation loop without the cavitation device and is included in Section S2 of the supplementary information. While solving the PBM, the volume fraction of each of the groups of drop sizes at the circulation inlet was specified by calculating the mass-averaged volume fraction of the corresponding group at the outlet as:

$$\gamma_{k,in} = \left[\frac{\sum_i v_i A_i \rho_i \gamma_{ki}}{\sum_i v_i A_i \rho_i} \right] at \text{ outlet_circ} \quad (11)$$

where ρ_i is mixture density, v_i and A_i are velocity of the mixture in the cell i and the area of the cell i , respectively, and γ_{ki} is the bin fraction of k^{th} size group in the cell i at the outlet. The summation sign indicates summing over all the computational cells at the outlet. After achieving a

steady state solution of the $PBEs$, the outlet $DSDs$ were analysed and compared with the experimental data. The probability density function (PDF) was calculated by dividing $\gamma_{O,i}$ with the width of the group i (Δx_i) as ($PDF = \gamma_{O,i}/\Delta x_i$). The simulated DSD results are discussed in Section 4.

3.4. Solution of model equations

The cavitating flow simulations were performed using the multi-phase mixture model in Ansys Fluent 2024R1 by solving the mixture phase continuity and momentum equations, along with volume fraction transport equations for the secondary phases. The meshing was performed using the Ansys Mosaic meshing technique, which resulted in hexahedral elements in the region of interest (central region of the vortex chamber). The first cell height was maintained at 0.02 mm, which resulted in a y^+ value of less than 5. Region-specific refinement areas were defined by using a body of influence (BOI) approach to capture the dynamics in relevant areas of the domain. Additional details of meshing and images of the mesh generated are included in Section S2 of the supplementary information. The grid sizes used were based on the grid independence study performed by Gode et al (Gode et al., 2023). The SIMPLE algorithm was used to couple the pressure and velocity. The momentum, turbulent kinetic energy, specific dissipation rate and density were spatially discretized using the second order upwind scheme. The pressure was discretized using a PRESTO! Scheme. A transient formulation was used to account for the unsteady nature of the flow. The default under-relaxation factors 0.3, 0.7, 0.8 and 0.5 for pressure, momentum, energy, turbulence quantities, and density, respectively, were used. The convergence at a particular time step was achieved by performing 30 iterations per time step.

The approach for simulating a circulation loop setup was validated using pressure drop versus flow rate data for water as the working fluid. The setup used for obtaining the experimental data of pressure drop versus flow rate was the same as shown in Fig. 1, with both the inlet pumps being used for water. Fig. 4 shows the comparison of simulation results with experimental data, and it is observed that the maximum difference between simulation and experimental data does not exceed 5 %, indicating the validity of the applied simulation methodology for the circulation loop.

The PBM simulations were decoupled from the flow simulations and solved using a steady state approach. The decoupling was used based on published data (Thaker and Ranade, 2022) which showed that the differences between the coupled and decoupled approaches were insignificant. The population balance equation was solved by representing the droplet population by a finite number of bins over the range of 0.1–750 μm . The in-built solver available within ANSYS Fluent was used for this purpose. For the PBM simulations, the influence of number of bins considered for representing the droplet population was examined by Thaker and Ranade (2023a) for 20, 40 and 80 bins. Based on their

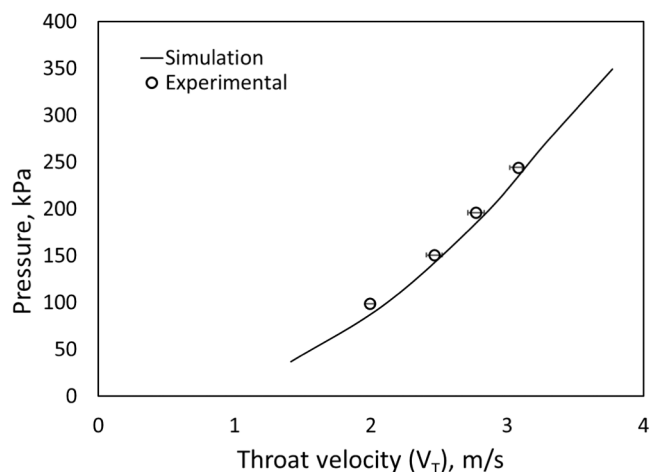


Fig. 4. Comparison of experimental and simulation pressure drop data.

results, 20 bins were finalised for all subsequent simulations. The first order convective numerical scheme was used for solving the bin fraction. The PBM equations were solved till convergence, which was determined by residual criteria (10^{-6}) as well as monitoring the change in outlet Sauter mean diameter (% change < 1%). The *DSD* of the emulsion was obtained by recording the bin fraction values for different bin sizes at the outlet boundary.

3.5. Overall strategy of CFD+PBM+ANN ensemble approach

An overview of the ensemble approach used in this work is shown in Fig. 5 and described here. This ensemble approach integrates device-scale CFD, micro-scale cavity dynamics (via the ANN based surrogate model), and the population balance model (PBM) for predicting *DSD* and characteristic diameters of emulsions produced continuously using VD. The device-scale CFD simulations are performed to predict the cavitation zone inside a vortex-based HC device operated in continuous mode. The inputs to the CFD model were emulsion flow rate, oil volume fraction, and flow rate ratio (or total flow rate through the device). The resulting flow field from CFD simulation served as an input to the PBM simulations, while the distribution of vapour volume fraction in the domain was used to identify the effective cavitation zone, defined using $\alpha_{vc} \leq \alpha_v < 0.6$. The ability of ANN to estimate the localised, high energy dissipation rates resulting from cavity collapse is harnessed to simulate device scale droplet breakage. The inputs to the ANN-based surrogate model for cavity dynamics were obtained from the characteristic flow features in the effective cavitation zone. The local volume-averaged values of pressure (P_{cz}), turbulence kinetic energy (k_{cz}) and specific dissipation rate (ω_{cz}) in the cavitation zone were used to obtain the corresponding ANN model inputs, pressure (P_{cz}), amplitude of

pressure fluctuations (P_{cz}^a), frequency of pressure fluctuations in the cavitation zone (f_{cz}), respectively (using Eqs. 3–5). Using the initial cavity radius as a model parameter, the combined CFD+ANN model was used to estimate energy dissipation rates generated by collapsing cavities (ϵ_{cav}). The turbulent energy dissipation rate due to cavitation (ϵ_{cav}) was incorporated in the breakage model by Alopaeus et al. (2002) and used for solving breakage due to cavitation phenomena in the effective cavitation region whereas the distribution of ϵ obtained from the flow simulations was used in the rest of the domain for modelling breakage due to turbulent shear (Eq. (6)). Finally, the PBM outputs the *DSD* at the outlet, which is processed for characteristic diameters. This ensemble approach based on CFD+ANN+PBM realises a robust and systematic framework for simulating droplet breakage while minimising non-physical adjustable parameters.

4. Results and discussion

4.1. Experimental data for continuous emulsion production

The continuous oil-in-water emulsion production experiments were carried out for different pressure drop and flow rate ratio (Q_D/q_{net}) values at a constant oil fraction of 0.05. The *DSD* and characteristic diameter values obtained from continuous experiments were compared with batch experiments to check the performance of the continuous process as compared to its batch counterpart. Fig. 6 provides a comparison of batch and continuous modes for emulsion production for a pressure drop value of 250 kPa. The data for batch experiments are obtained from the recent works of Thaker and Ranade (2023a). The flow rate ratio (Q_D/q_{net}) in a continuous experiment can be considered equivalent to the number of passes through the device in a batch experiment (Gode et al., 2024). From Fig. 6, it can be inferred that the *DSD* obtained is independent of the mode of operation. The two peaks in *DSD* indicate the presence of a cavitation mechanism for droplet breakage as discussed by Thaker and Ranade (2023a) and Gode et al. (2024) and discussed above in Section 3.1.

For continuous emulsion production, the influence of the flow rate ratio (Q_D/q_{net}) on resulting *DSD* was investigated for different pressure drop values. Fig. 7 shows the influence of pressure drop on *DSD* and d_{32} values. With increase in pressure drop value the intensity of cavitation increases leading to increased height of first peak indicating prominence of cavitation induced breakage over droplet breakage due to turbulent shear. This is also observed in the Sauter mean diameter (d_{32}) values plotted as function of q_{net} for varying pressure drop values. The first peak (with smaller mean droplet size) is due to droplet breakage in the cavitation zone, and the second peak represents droplets that bypass the effective cavitation zone and experience relatively low shear forces in the bulk flow. The prevalence of second peak at steady state indicates that the larger droplets do not encounter sufficiently high energy dissipation rate to break them further. This phenomenon is a direct result of the non-uniform turbulent flow inside the vortex-based device.

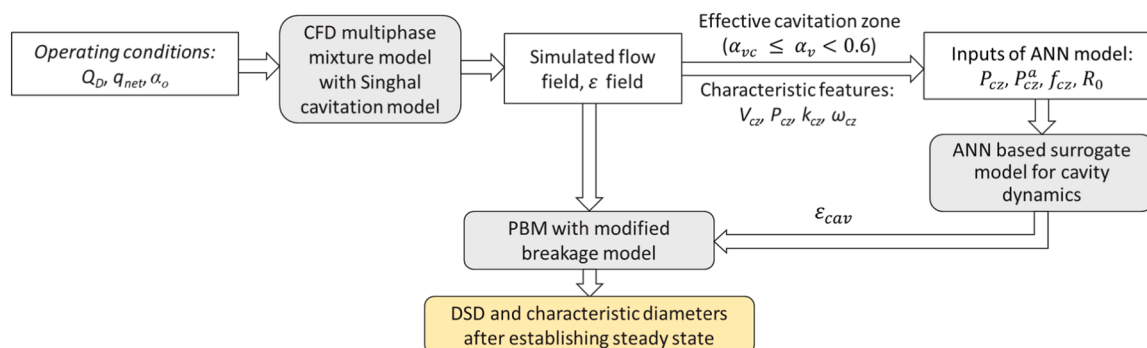


Fig. 5. Flowchart showing the ensemble approach.

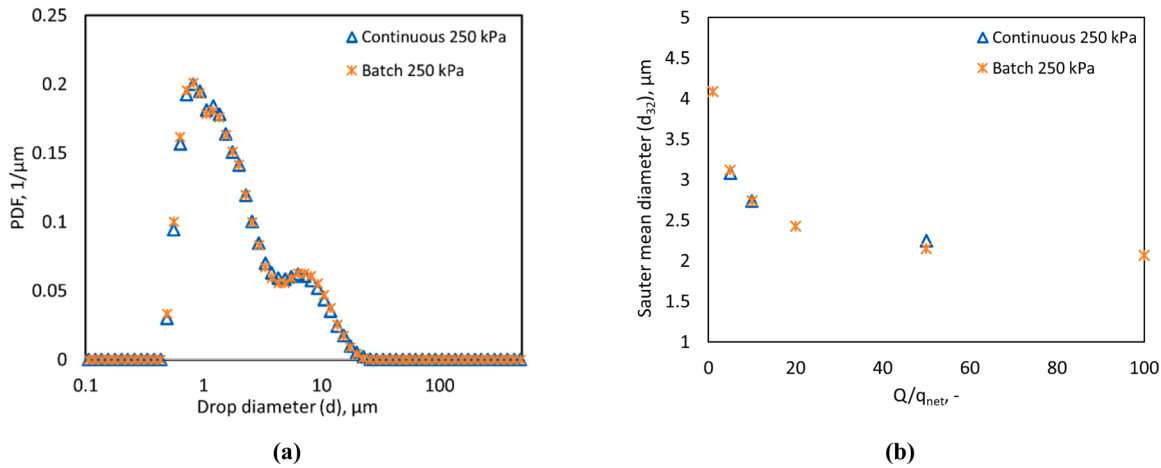


Fig. 6. Comparison of (a) DSD (at n_p = 50) and (b) Sauter mean diameter (d₃₂) for continuous and batch modes of operation at ΔP = 250 kPa.

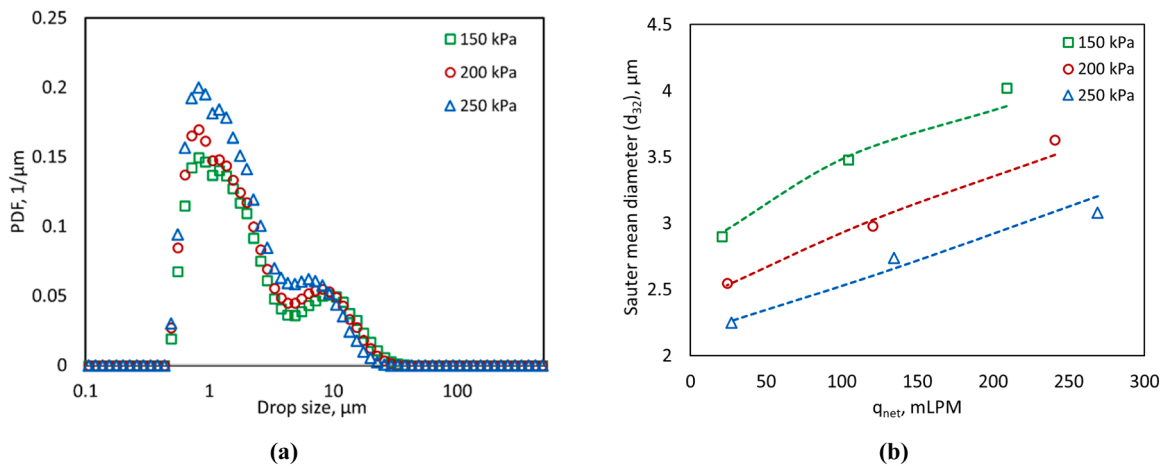


Fig. 7. Droplet size distribution and the Sauter mean diameter (a) Influence of pressure drop across the device at constant flow rate ratio (at Q_D/q_{net} = 10) and (b) Influence of flow rate of emulsion (q_{net}) at different pressure drops across the device. The dashed lines represent the d₃₂ values obtained from Eqs. (12) to (15).

If all large droplets encounter the high turbulent dissipation rate cavitation zone, the system will tend towards a monomodal distribution. As the flow rate ratio increases – that is effectively droplets pass through the device multiple times, the size of the second peak representing larger droplets decreases and eventually DSD becomes mono-modal (Thaker and Ranade, 2023a). The variation in DSD with flow rate ratio for different values of pressure drop is shown in Figure S10 of the supplementary information. This further exemplifies the possibility of approach to mono-modal distribution with increase in flow rate ratio.

The experimental data of d₃₂ may be represented as a function of Q_D/q_{net} as:

$$d_{32} = d_{\min} + (d_0 - d_{\min})e^{-\left(\frac{Q_D}{q_{net}}\right)^\varphi} \quad (12)$$

Where d_{min} is the minimum Sauter mean diameter at very high value of Q_D/q_{net} which is equivalent to a low emulsion flow rate value for a particular value of pressure drop (or Q_D). The maximum Sauter mean diameter, d₀, is the value of Sauter mean diameter at very small value of (Q_D/q_{net}). The value of d₀ was found to be 4.5 μm. φ may be regarded as a per-pass breakage parameter which is a characteristic of a device design and operating conditions.

This minimum Sauter mean diameter may be expressed as a function of mean energy dissipation rate as:

$$d_{\min} = 33 (\bar{\epsilon})^{-1/3} \mu m \quad (13)$$

Where $\bar{\epsilon}$ is the mean energy dissipation rate for the vortex-based emulsification device, which is given by the relation:

$$\bar{\epsilon} = \frac{\Delta P}{\rho_m} \frac{Q_D}{V_D} \frac{m^2}{s^3} \quad (14)$$

where ΔP is pressure drop across the device and Q_D is the flow rate through the device.

The per-pass breakage parameter, φ was found to be related to the mean energy dissipation rate as:

$$\varphi = \varphi_m (1 - e^{-\beta \bar{\epsilon}}) \quad (15)$$

Where φ_m is maximum value of φ and β is a fitted parameter. The values of φ_m and β were found to be 0.3 and 2.75 × 10⁻⁴ (s³/m²) respectively. For the limiting case, Q_D/q_{net} = 1, the d₃₂ value approaches the limiting Sauter mean diameter value, d₀ = 4.5 μm. It can be seen from Fig. 7b that the fit based on Eqs. (12) to (15) represent the experimental data quite well. The relation between d₃₂ and emulsion flow rate (q_{net}) provides a basis for determining the specific operating conditions (ΔP or Q_D value) for obtaining an emulsion with desired d₃₂ and at the flow rate q_{net}. This experimental data was further used for evaluating the computational models. The CFD+PBM+ANN simulations for predicting DSD of emulsions were carried out at five operating conditions for

comparing the results with experimental data: first, for a constant emulsion flow rate of 120 mLPM, the flow through the device (Q_D) was selected such that the pressure drop values were 150, 200 and 250 kPa and secondly for a constant pressure drop value of $\Delta P = 200$ kPa, the emulsion flow rate was varied as 24, 120 and 240 mLPM. The comparison of the simulated results with the experimental data is preceded by the results of the sensitivity study considering two key model parameters, namely critical vapour volume fraction (α_{vc}) and initial cavity radius (R_0) as discussed in the following Section 4.2.

4.2. Sensitivity study of α_{vc} and R_0 for DSD estimation

The CFD+PBM+ANN methodology presented in Section 3.2 for including the effect of collapsing cavities on droplet breakage was used to examine the influence of R_0 and α_{vc} on the simulated DSD. In the first step, a steady state flow field was simulated using the CFD model. These flow results were used to obtain the input parameters for the ANN model. The influence of variation in α_{vc} on the ANN model input parameters for different operating conditions were studied. Fig. 8 shows the influence of α_{vc} on the values of key input parameters (P_{cz} , P_{cz}^a and f_{cz}) of the ANN model for estimating ε_{cav} for different pressure drops across the HC device ($\Delta P = 150, 200$ and 250 kPa). It can be seen from Fig. 8 that, decreasing the size of the effective cavitation zone (that is, increasing the value of α_{vc}), the P_{cz} value decreases with the value moving closer to the vapour pressure. Similar behaviour was observed for different pressure drop values. The change in cavitation zone pressure (P_{cz}) was observed to be less for α_{vc} greater than or equal to 0.1 indicating that beyond this value the pressure value becomes almost

independent of the cavitation zone. The value of P_{cz} corresponding to $\alpha_{vc} \geq 0.1$ is of the order of vapour pressure. This is the pressure experienced by the cavity after it travels a very short distance before collapsing. The amplitude of pressure fluctuations (P_{cz}^a) was observed to decrease with an increase in α_{vc} value or reduction in the effective cavitation zone, whereas the frequency of pressure fluctuations (f_{cz}) showed an increase when the effective cavitation zone was reduced.

It can be seen that some of the ANN input parameters are very sensitive to the value of α_{vc} when $\alpha_{vc} < 0.1$. Fortunately, the probability of encounter between a droplet and a collapsing cavity may reduce significantly when $\alpha_{vc} < 0.1$. Considering this and to avoid undue sensitivity to the parameter α_{vc} the values of $\alpha_{vc} = 0.1$ and 0.2 were considered for further investigation.

The ANN simulations were performed to obtain the value of ε_{cav} for two values of $\alpha_{vc} = 0.1$ and 0.2 at varying values of initial cavity radius. As discussed in Section 3.2, the value of α_{vc} defines the effective cavitation region where the probability of cavities encountering oil droplets is high. The droplet breakage in the effective cavitation zone is predominantly due to high localised energy dissipation rates generated by collapsing cavities. The initial cavity radius impacts the cavitation intensity and hence the value of ε_{cav} . The ε_{cav} values obtained for different pressure drop values are shown in Fig. 9 at two values of α_{vc} (0.1 and 0.2) over a range of initial cavity radius. The trends observed for $\alpha_{vc} = 0.1$ and 0.2 are similar. Considering the monotonous behaviour of ε_{cav} with respect to the initial cavity radius exhibited by the case of $\alpha_{vc} = 0.1$, possibility of using a larger range of R_0 and a lower possibility of encounter between droplets and collapsing cavities, the lower limit of vapour volume fraction used for identifying the effective cavitation

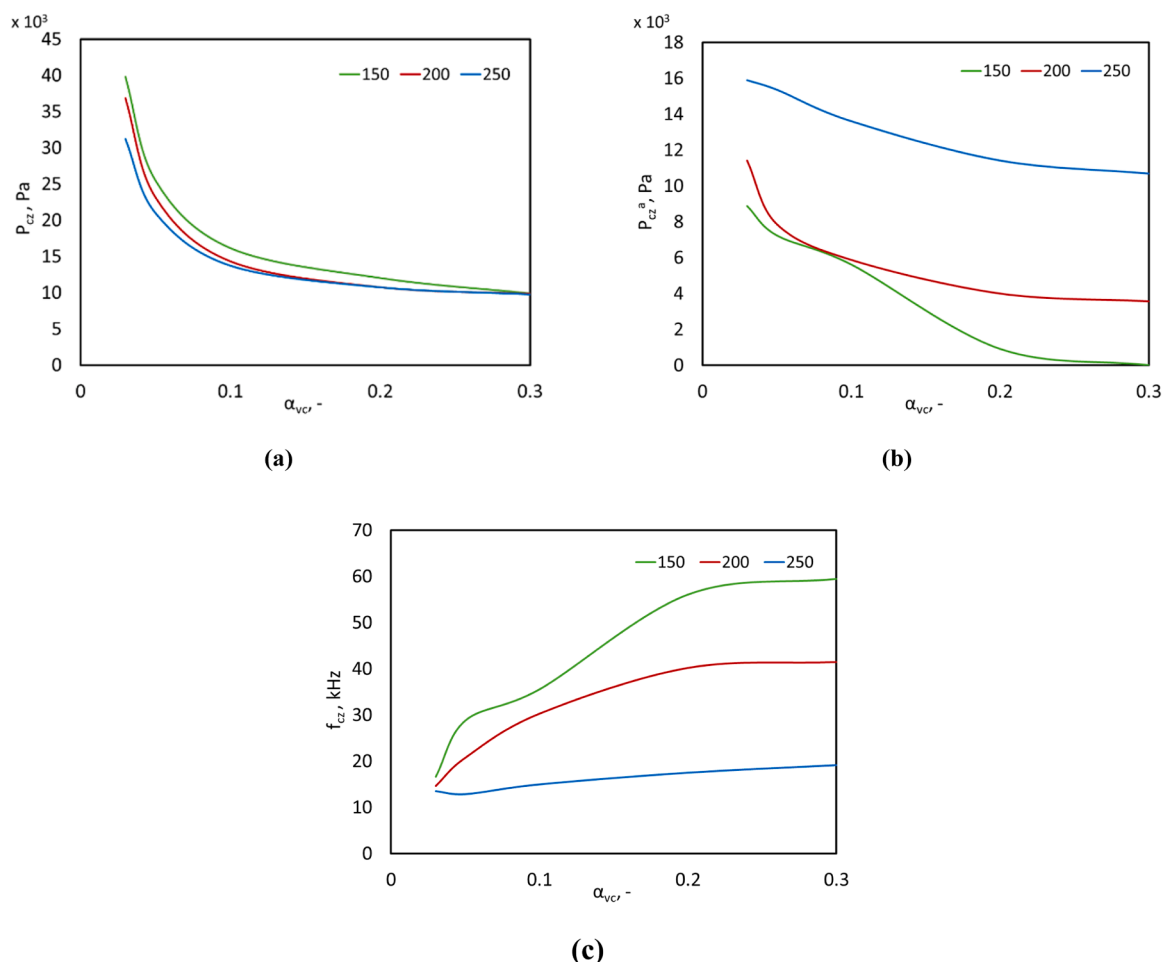


Fig. 8. Influence of α_{vc} on (a) P_{cz} (b) P_{cz}^a and (c) f_{cz} for operating conditions $\Delta P = 150, 200$ and 250 kPa and $Q_D/q_{net} = 10$.

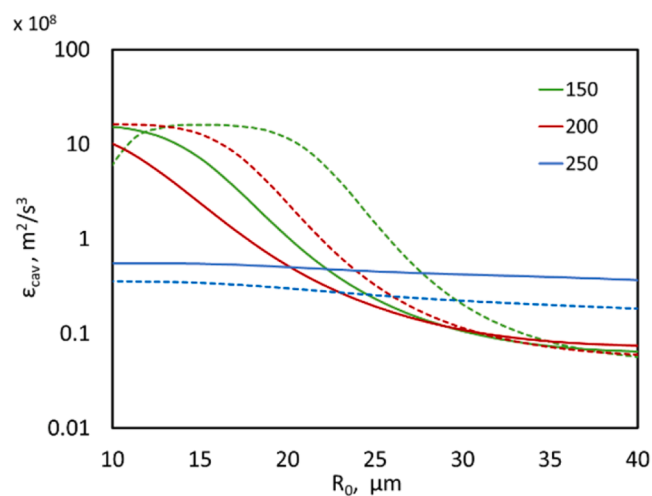


Fig. 9. Influence of R_0 on predicted ϵ_{cav} at pressure drop values of $\Delta P = 150$, 200 and 250 kPa at $\alpha_{vc} = 0.1$ shown by solid lines and $\alpha_{vc} = 0.2$ shown by dashed lines.

region, α_{vc} , was set to 0.1 for subsequent simulations.

With the value of α_{vc} fixed, the sensitivity of initial cavity radius on DSD prediction for varying operating conditions was investigated. PBM simulations were performed with the modified approach discussed in Section 3.4 for different values of R_0 and predicted DSD and characteristic diameters compared with experimental (Fig. 10) for different pressure drop values. The Alopaeus et al. model parameters, C_2 , C_3 and C_4 (Eq. 6) were maintained the same as reported by Thaker and Ranade (2023a). The sensitivity study results obtained for $\Delta P = 200$ kPa and $Q_D/q_{net} = 10$ are shown in Fig. 10 (results for $\Delta P = 150$ and 250 kPa are included in Section S3 of supplementary information). A lower value of R_0 resulted in higher concentration of cavities for the same pressure fluctuations leading to higher values of localised energy dissipation rates ϵ_{cav} . This is evident from Fig. 10a which indicates that decreasing the R_0 value leads to the DSD shifting towards finer droplet sizes with an increase in the height of the first peak. The location of the second peak with larger mean droplet diameter is unaltered and the height of the second peak increases with an increase in R_0 value. The initial cavity radius is the most important physical parameter that defines the conditions for subsequent cavity collapse and thus the energy dissipation rate due to cavitation. A smaller initial cavity could be considered as being more rigid and as it travels from low pressure region into a higher pressure region in the bulk, it has less inertia to overcome leading to a

more violent implosion. Comparing this with a larger initial cavity, that has higher volume of vapour and non-condensable gas, the collapse of the cavity leads to lower values of energy dissipation rates as the collapse is cushioned by the gas/vapour present inside the cavity. The comparison of simulated and experimental DSD indicates that for $\Delta P = 200$ kPa, the R_0 value is between 10 and 20 μm . The influence of R_0 on predicted characteristic diameters for $\Delta P = 200$ kPa and $Q_D/q_{net} = 10$ is shown in Fig. 10b. The D_{10} and d_{32} values increase with an increase in R_0 and cross the experimental values for R_0 between 10 and 20 μm . Additional results from the sensitivity study for pressure drop values, $\Delta P = 150$ and 250 kPa, are included in Section S3 of the supplementary information.

Based on the sensitivity study, the initial cavity radius R_0 was fixed at 17 μm . This initial cavity radius value was used for predicting DSD for cases with varying ΔP and q_{net} and the DSD and characteristic diameter values obtained were compared with experimental data.

The influence of daughter size distribution functions on simulated DSD s was studied to affirm the selection of parabolic distribution. The results from this study are now included in the supplementary information Section S4. This study indicated that the widely used parabolic daughter size distribution can reasonably simulate the DSD s generated by the combined action of shear and cavitation. Considering the difficulties in capturing an ultra-fast dynamic of collapsing cavities and their interaction with suspended oil droplets, adequate data required for formulating the daughter size distribution generated by cavitation is not available. Based on the sensitivity study and in the absence of relevant data for formulating the daughter size distribution, in this work, we used the most commonly used symmetric parabolic daughter size distribution.

4.3. Comparison of simulated and experimental DSD for continuous emulsification

The results obtained using the CFD+PBM model for the continuous set-up operated at the pressure drop values of 150, 200 and 250 kPa were used to calculate key quantities needed for estimating ϵ_{cav} using ANN as discussed earlier. The effective cavitating region was seen to increase with an increase in pressure drop values, as shown in Figure S5 of the supplementary information. The change in flow rate ratio value led to an insignificant change in the flow and effective cavitating region (see Figure S6 of supplementary information). This is largely due to the pressure drop value remaining same in the device.

CFD simulation results of effective cavitation zone, mean pressure, turbulent kinetic energy and specific energy dissipation rates averaged over the effective cavitating zone are listed in Table S1. These values

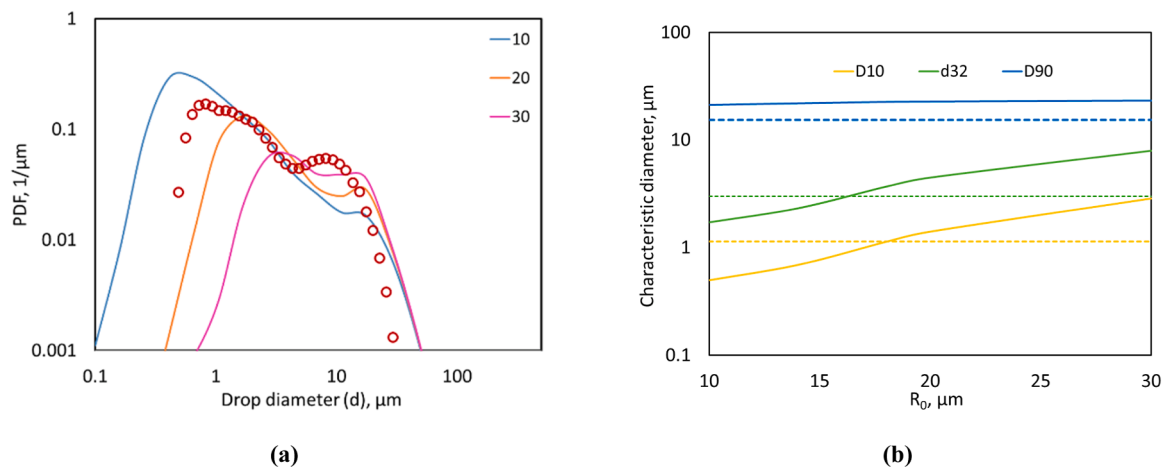


Fig. 10. Influence of R_0 on predicted (a) DSD and (b) Characteristic diameters (D_{90} , d_{32} and D_{10}) for $\Delta P = 200$ kPa and $Q_D/q_{net} = 10$. Experimental DSD is shown as symbols and simulated results as solid lines, and dashed lines represent experimental characteristic diameter values.

were used to calculate the parameters needed for the ANN model. These parameters are listed in Table S2. In addition to the parameters derived from the CFD simulations, it is essential to set the initial cavity radius, R_0 . Based on the sensitivity results discussed in Section 4.2, the initial cavity radius for all three pressure drop values was set to $17 \mu\text{m}$. The comparison of predicted *DSD* and characteristic diameters with experimental for pressure drop values of 150, 200 and 250 kPa using the modified Alopaeus et al. breakage model and initial cavity radius R_0 as $17 \mu\text{m}$ are shown in Fig. 11. The predicted *DSD* was observed to be bimodal, as seen in experiments where the first peak corresponds to breakage due to cavitation, and the location and height of the second peak indicate droplet breakage from turbulent shear. The simulated *DSD* for $\Delta P = 150 \text{ kPa}$ shows a qualitatively good match with the experimental *DSD*, however, exhibits a deviation in the comparison of the characteristic diameters. The predicted values of characteristic diameters are higher as compared to the experimental ones for $\Delta P = 150 \text{ kPa}$. The height of the first peak corresponding to the cavitation induced droplet breakage was observed to increase with an increase in pressure drop value, and the height of the second peak decreased with an increase in pressure drop for both predicted and experimental *DSD*. The second peak height and location indicative of breakage due to turbulent shear predicted by simulations were seen to deviate from the experimental one, with the spread of the predicted *DSD* being more as compared to the experimental results. This was also observed in the predicted *D90* values. The predicted *DSD* and characteristic diameters agree reasonably well with the experimental data for pressure drop values of 200 and 250 kPa.

The use of a constant initial cavity radius captures the nature of the *DSD* reasonably well over the range of pressure drop values considered. The quantitative differences observed at a lower pressure drop value of 150 kPa indicate that a lower value of initial cavity radius could be applied for this case to obtain a quantitative match with experimental data.

The comparison of *DSD* and characteristic diameters (d_{32} , *D10* and *D90*) obtained for $\Delta P = 200 \text{ kPa}$ and varying $q_{net} = 240, 120$ and 24 mLPM ($Q_D/q_{net} = 5, 10$ and 50) using the initial cavity radius value ($R_0 = 17 \mu\text{m}$) is shown in Fig. 12. The predicted *DSDs* for all q_{net} values show reasonably good agreement with the experimental data. The location and height of the first peak were predicted correctly, while some deviations were observed with respect to the location and height of the second peak (see Table S3 and Table S4 of supplementary information). The first peak corresponding to breakage due to cavitation phenomena was observed to be well predicted with the approach presented in this work. The d_{32} and *D10* values show a reasonable agreement with the experimental results obtained with varying emulsion flow rate over one order of magnitude (for $q_{net} = 240, 120$ and 24 mLPM). The predicted *D90* was higher for all the three cases simulated as the spread of the predicted *DSD* was more compared to experimental results and the predicted drop diameter corresponding to the second peak of the *DSD* was higher than experimental data.

The difference between the predicted and experimental characteristic diameters may be reduced by considering variation of R_0 with pressure drop and flow rate ratio (Q_D/q_{net}). Fig. 13 shows the results obtained by using different values of R_0 . For 150 kPa pressure drop case,

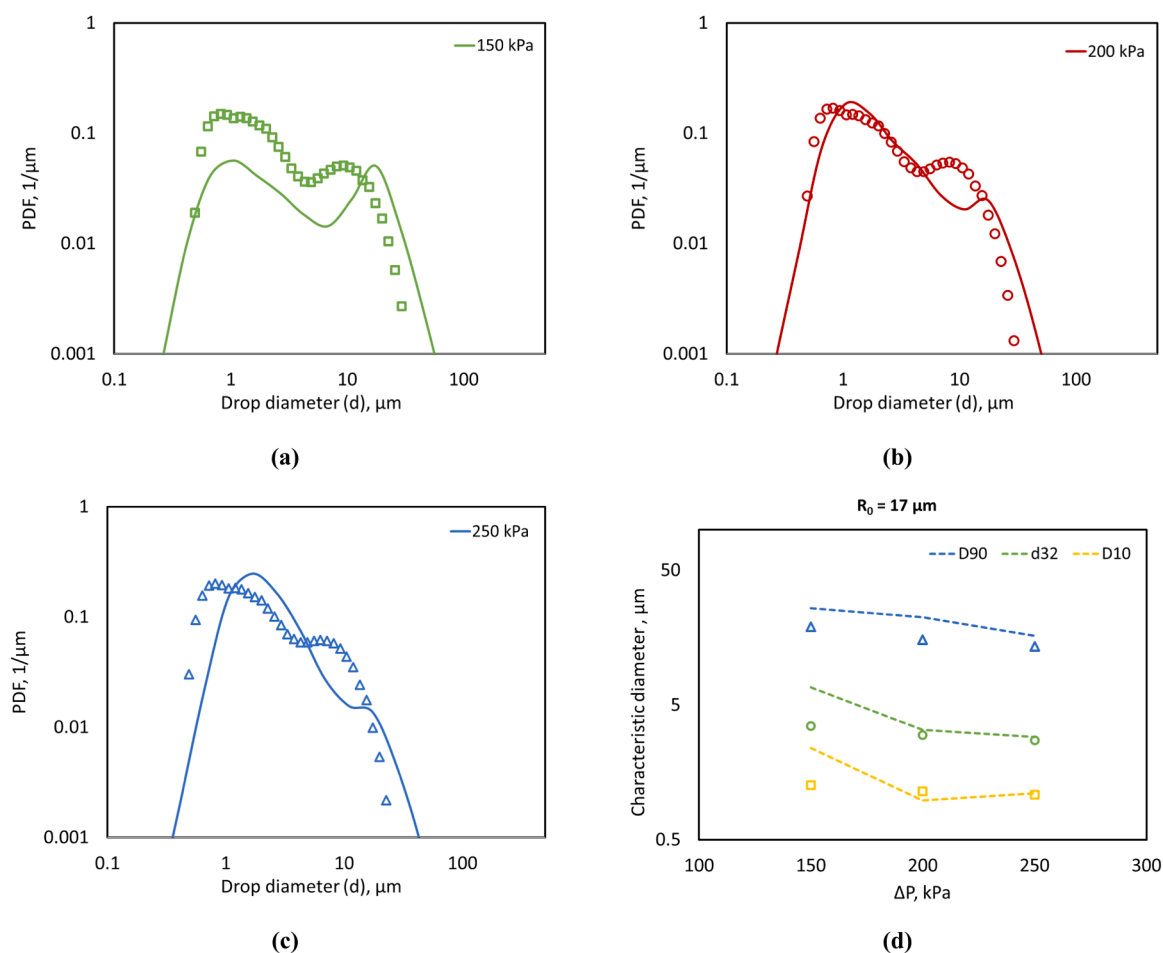


Fig. 11. Comparison of simulation and experimental *DSD* at pressure drop value (a) $\Delta P = 150 \text{ kPa}$, (b) $\Delta P = 200 \text{ kPa}$ and (c) $\Delta P = 250 \text{ kPa}$ and (d) Characteristic diameters (*D90*, d_{32} and *D10*) for varying pressure drop values and $Q_D/q_{net} = 10$. Experimental data are shown as symbols, and simulation results are shown as solid lines for *DSD* and dashed lines for characteristic diameter.

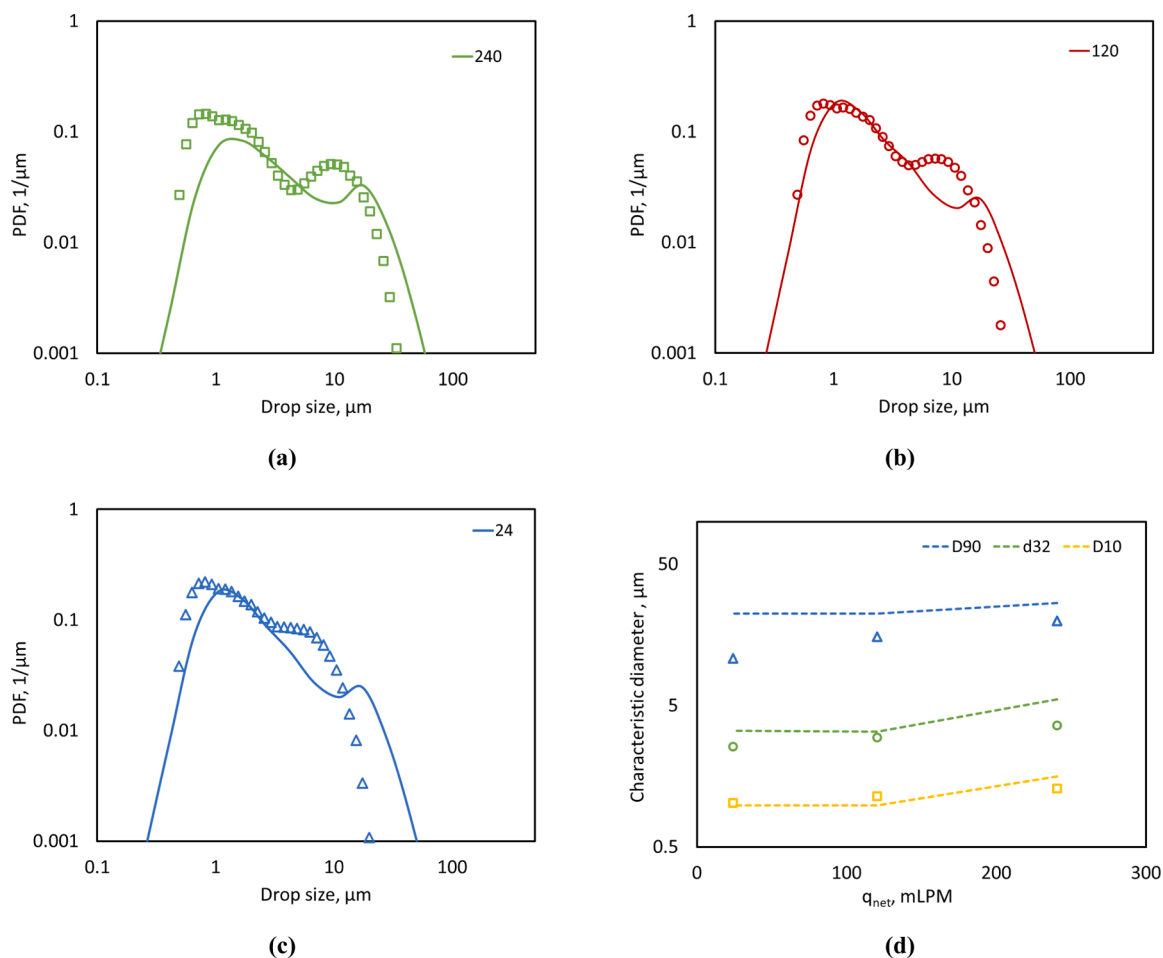


Fig. 12. Comparison of simulation and experimental DSD at (a) $q_{net} = 240$ mLPM, (b) $q_{net} = 120$ mLPM and (c) $q_{net} = 24$ mLPM and (d) Characteristic diameters (D90, d_{32} and D10) for $\Delta P = 200$ kPa and varying q_{net} values. Experimental data are shown as symbols, and simulation results are shown as solid lines for DSD and dashed lines for characteristic diameter.

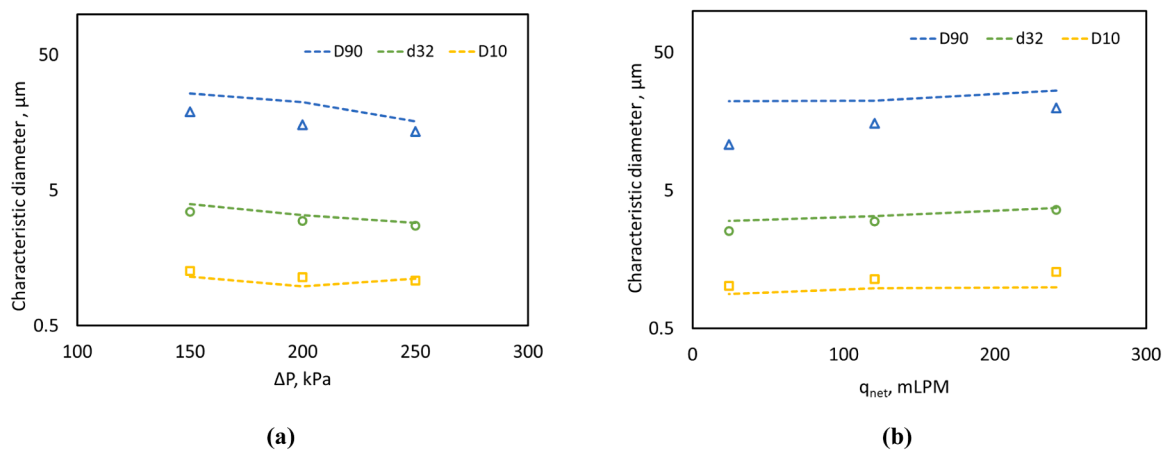


Fig. 13. Comparison of simulation and experimental characteristic diameters (D90, d_{32} and D10) at (a) Varying pressure drop values and (b) Varying q_{net} values. Experimental data are shown as symbols and simulation results are shown as solid lines.

the R_0 value was reduced to $12 \mu\text{m}$ and the R_0 value used for varying flow rate ratio were $R_0 = 12$ for $Q_D/q_{net} = 5$ and $R_0 = 15$ for $Q_D/q_{net} = 50$.

The presented approach of using CFD+PBM coupled with ANN based surrogate model for cavity dynamics can predict the DSD and characteristic diameters of emulsions produced continuously. This study shows

that for emulsions produced using hydrodynamic cavitation devices, it is imperative to include droplet breakage due to cavitation to obtain a bimodal DSD as observed in experiments. This was achieved by incorporating a localised high value of turbulent dissipation rate in the cavitating region. The use of ANN based cavity dynamics model to obtain representative values of localised turbulent dissipation rate

builds confidence in the approach adopted. The key ANN model input parameters used for obtaining ε_{cav} values for different simulations performed to validate the approach are tabulated in [Tables S1 and S2 of supplementary information](#). These input parameters are indicative of the flow characteristics in the device at different operating conditions. Some key observations are outlined here: The effective cavitation volume increased (almost exponentially) with pressure drop across the HC device. Mean pressure and turbulent kinetic energy (amplitude of pressure fluctuations) also increase with increase in pressure drop. The frequency of pressure fluctuations in the cavitation zone was found to be inversely proportional to the pressure drop value. For a constant pressure drop, the net flow rate does not influence the effective cavitation zone volume, mean pressure and turbulent kinetic energy since the flow is dominated by the value of circulatory flow through the device (Q_D) than the relatively small value of net flow rate (q_{net}). For obtaining good agreement with the observed *DSD* and characteristic diameters, the initial cavity radius, R_0 is almost linearly proportional to the pressure drop across the device. These observations provide useful guidance for understanding influence of operating conditions on resulting *DSD*.

The current work presents a novel ensemble approach that integrates device-scale CFD, micro-scale cavity dynamics (via the ANN based surrogate model), and the Population Balance Model (PBM) for predicting droplet size distribution (*DSD*) and characteristic diameters of emulsions produced continuously using a vortex based hydrodynamic cavitation device. This approach is developed to harness the ability of the ANN model to estimate the localised, high energy dissipation rates resulting from cavity collapse for simulating device scale processes. This approach is implemented to provide a systematic and robust framework that minimises the reliance on non-physical adjustable parameter. The presented characteristics of the cavitation zone and the ensemble approach would be useful for simulating other processes beyond droplet breakage.

5. Conclusions

The continuous production of rapeseed oil-in-water emulsions was studied experimentally to obtain the influence of flow rate ratio (Q_D/q_{net}) and pressure drop (ΔP) on *DSD* and characteristic diameters. The CFD simulation methodology used for mimicking a continuous setup for emulsion production is developed and validated by comparing simulation results with experimental data of pressure drop versus flow rate. An ensemble approach based on CFD, PBM and ANN was developed and used for predicting *DSD* of emulsions produced in a continuous mode of operation using VD. The device-scale CFD simulations are used to predict the cavitation zone and relevant input parameters needed for the ANN model, namely, mean pressure, pressure fluctuation amplitude and frequency and temperature. Using the initial cavity radius as a model parameter, the combined CFD+ANN model is used to estimate energy dissipation rates generated by collapsing cavities. This estimated energy dissipation rates are then used in the breakage kernel of PBM to simulate droplet breakage. The following are the key findings from this study:

- The *DSD* of oil-in-water emulsions produced using vortex-based HC device showed a bimodal nature. The *DSD* moved towards monomodal with increase in flow rate ratio Q_D/q_{net} .
- A unified correlation is developed to estimate the Sauter mean diameter d_{32} as a function of pressure drop across VD and the flow rate ratio Q_D/q_{net} (Eq. (12)). The predictions from the developed correlation agree with the experimental data very well (Fig. 7b).
- An approach to model continuous production of emulsions by considering a small section of the circulation loop as solution domain was presented and validated.
- An ensemble approach based on CFD, PBM and ANN which accounts for the influence of cavitation on droplet breakage was developed. The effective cavitation region was found to be a region having vapour volume fraction between 0.1 and 0.6 ($0.1 \leq \alpha_{vc} < 0.6$). A

typical range of initial cavity radius needed for estimating localised energy dissipation rates caused by collapsing cavities was found to be in the range of 10–20 μm .

- Assumption of a constant initial cavity radius over the range of considered pressure drops ($\Delta P = 150$ to 250kPa) and emulsion flow rates ($q_{net} = 24$ to 240) lead to reasonable agreement between the predicted and experimental results. If the initial cavity radius is varied as a function of pressure drop or flow rate ratio, the agreement between the predicted and experimental results was improved.

The presented ensemble approach based on CFD, PBM and ANN will be useful simulating influence of design and operating parameters on *DSD* of emulsions produced using HC devices.

CRedit authorship contribution statement

Amol Gode: Writing – original draft, Methodology, Investigation, Formal analysis, Data curation. **Vivek V. Ranade:** Writing – review & editing, Validation, Supervision, Software, Resources, Project administration, Methodology, Funding acquisition, Conceptualization.

Declaration of Competing Interest

The authors declare that they have no known competing financial interests or personal relationships that could have appeared to influence the work reported in this paper.

Acknowledgements

The authors greatly acknowledge the support provided by Ansys for CFD licence under an academic partnership programme. The authors greatly acknowledge the financial support by Taighde Éireann–Research Ireland (Project ID: 20/FFP-A/8518). The authors also wish to acknowledge the Irish Centre for High-End Computing (ICHEC) for the provision of computational facilities and support. The authors thank Abhijeet Thaker for assisting with the experimental setup and providing valuable inputs for simulations.

Appendix A. Supporting information

Supplementary data associated with this article can be found in the online version at [doi:10.1016/j.cherd.2025.11.010](https://doi.org/10.1016/j.cherd.2025.11.010).

References

- Alopaevs, V., et al., 2002. Simulation of the population balances for liquid–liquid systems in a nonideal stirred tank. Part 2—parameter fitting and the use of the multiblock model for dense dispersions. *Chem. Eng. Sci.* 57 (10), 1815–1825.
- Ansys® Academic Research Mechanical and CFD, Release 2020 R1, Help System, *Fluent Theory Guide*, ANSYS, Inc.
- Athavale, M., et al., 2002. Application of the full cavitation model to pumps and inducers. *Int. J. Rotating Mach.* 8.
- Bachnak, R., et al., 2024. Influence of aqueous phase salt and oil phase surfactants and viscosity on the dynamic interfacial tension and coalescence timescales. *J. Phys. Chem. B* 128 (44), 10986–10998.
- Bagkeris, I., et al., 2019. Simulation of turbulent emulsification in a sonolator mixer: interpretation of drop breakage time. *Chem. Eng. Technol.* 42 (8), 1555–1565.
- Becker, P.J., et al., 2014. Coupled population balance–CFD simulation of droplet breakup in a high pressure homogenizer. *Comput. Chem. Eng.* 68, 140–150.
- Calvo, F., et al., 2024. A population balance model for cosmetic emulsion design: A multiscale approach. *Chem. Eng. Sci.* 287, 119737.
- Carpenter, J., et al., 2022. Critical review on hydrodynamic cavitation as an intensifying homogenizing technique for oil-in-water emulsification: theoretical insight, current status, and future perspectives. *Ind. Eng. Chem. Res.* 61 (30), 10587–10602.
- Carpenter, J., George, S., Saharan, V.K., 2017. Low pressure hydrodynamic cavitating device for producing highly stable oil in water emulsion: Effect of geometry and cavitation number. *Chem. Eng. Process. Process.Intensif.* 116, 97–104.
- Chen, T.Y., Chih-Cheng, Y., Ouyang, K., 2024. An experimental and numerical study on the cavitation and spray characteristics of micro-orifice injectors under low-pressure conditions. *Energies* 17, 1045.

- Dubbelboer, A., et al., 2014. Population balances combined with Computational Fluid Dynamics: a modeling approach for dispersive mixing in a high pressure homogenizer. *Chem. Eng. Sci.* 117, 376–388.
- Fathi Roudsari, S., et al., 2012. CFD modeling of the mixing of water in oil emulsions. *Comput. Chem. Eng.* 45, 124–136.
- Gode, A., Madane, K., Ranade, V.V., 2023. Design of vortex-based cavitation devices/reactors: influence of aspect ratio, number of inlets and shape. *Ultrason. Sonochem.* 101, 106695.
- Gode, A., Thaker, A.H., Ranade, V.V., 2024. Comparison of devices used for continuous production of emulsions: droplet diameter, energy efficiency and capacity. *Chem. Eng. Process. Process. Intensif.* 203, 109881.
- Håkansson, A., 2018. Rotor-stator mixers: from batch to continuous mode of operation—a review. *Processes* 6.
- Håkansson, A., 2020. Experimental methods for measuring the breakup frequency in turbulent emulsification: a critical review. *ChemEngineering* 4. <https://doi.org/10.3390/chemengineering4030052>.
- Håkansson, A., Rütten, E., Ranade, V.V., 2025. A CFD-based approach to study cavitation in high-pressure homogenizer valves. Part 2. Cavitation intensity. *Chem. Eng. Sci.* 121896.
- Hoekstra, A.J., Derksen, J.J., Van Den Akker, H.E.A., 1999. An experimental and numerical study of turbulent swirling flow in gas cyclones. *Chem. Eng. Sci.* 54 (13), 2055–2065.
- Islam, M.S., Ranade, V.V., 2025. Enhanced biomethane production via hydrodynamic cavitation pretreatment and co-digestion of brown and DAF sludge. *Water Sci. Technol.* 91 (9), 1032–1043.
- Janssen, J., Mayer, R., 2016. Computational Fluid Dynamics (CFD)-Based Droplet Size Estimates in Emulsification Equipment. *Processes* 4. <https://doi.org/10.3390/pr4040050>.
- Kamp, J., Villwock, J., Kraume, M., 2017. Drop coalescence in technical liquid/liquid applications: a review on experimental techniques and modeling approaches, 33 (1), 1–47.
- Laakkonen, M., Alopaeus, V., Aittamaa, J., 2006. Validation of bubble breakage, coalescence and mass transfer models for gas–liquid dispersion in agitated vessel. *Chem. Eng. Sci.* 61 (1), 218–228.
- Lebaz, N., Azizi, F., Sheibat-Othman, N., 2022. Modeling droplet breakage in continuous emulsification using static mixers in the framework of the entire spectrum of turbulent energy. *Ind. Eng. Chem. Res.* 61 (1), 541–553.
- Li, L., et al., 2023. A multiscale Eulerian–Lagrangian cavitating flow solver in OpenFOAM. *SoftwareX* 21, 101304.
- Liu, Z. and C. Brenner. *Models of cavitation event rate*. in *Proceedings of International Symposium of Cavitation, Deauville, France*. 1995.
- Liu, H., Yu, J., 2025. Investigation on stacked cavitation in rotational hydrodynamic cavitation reactor with a tapered rotor. *Chem. Eng. J.* 517, 164491.
- Maaß, S., Kraume, M., 2012. Determination of breakage rates using single drop experiments. *Chem. Eng. Sci.* 70, 146–164.
- Maindarkar, S.N., Hoogland, H., Henson, M.A., 2015. Achieving Target Emulsion Drop Size Distributions Using Population Balance Equation Models of High-Pressure Homogenization. *Ind. Eng. Chem. Res.* 54 (42), 10301–10310.
- Michael, V., Prosser, R., Kowalski, A., 2017. CFD-PBM simulation of dense emulsion flows in a high-shear rotor–stator mixer. *Chem. Eng. Res. Des.* 125, 494–510.
- Moholkar, V.S., Pandit, A.B., 2001. Modeling of hydrodynamic cavitation reactors: a unified approach. *Chem. Eng. Sci.* 56 (21), 6295–6302.
- Nakamoto, M., Tanaka, T., Yamamoto, T., 2017. Measurement of interfacial tension between oil and an aqueous solution via a floating drop method. *Colloids Surf. A Physicochem. Eng. Asp.* 529, 985–989.
- Ni, R., 2024. Deformation and breakup of bubbles and drops in turbulence. *Annu. Rev. Fluid Mech.* 56 (56, 2024), 319–347.
- Nie, L., et al., 2024. Comparative study of the cavitation situation and the non-cavitation situation under unsteady flow phenomena of a centrifugal pump. *J. Phys. Conf. Ser.* 2707 (1), 012054.
- O’Sullivan, J., et al., 2015. Comparison of batch and continuous ultrasonic emulsification processes. *J. Food Eng.* 167, 114–121.
- Panda, D., Saharan, V.K., Manickam, S., 2020. Controlled hydrodynamic cavitation: a review of recent advances and perspectives for greener processing. *Processes* 8 (2), 220.
- Pandare, A., Ranade, V.V., 2015. Flow in vortex diodes. *Chem. Eng. Res. Des.* 102, 274–285.
- Pandey, D.K., Thaker, A.H., Ranade, V.V., 2024. A simplified drop breakage model for emulsion-producing fluidic devices: application to fluidic oscillator, helical coil and vortex-based cavitation device. *Chem. Eng. Res. Des.* 205, 733–747.
- Pandit, A.V., Sarvothaman, V.P., Ranade, V.V., 2021. Estimation of chemical and physical effects of cavitation by analysis of cavitating single bubble dynamics. *Ultrason. Sonochem.* 77, 105677.
- Pang, H., Ngalle, G., 2021. Modeling of a valve-type low-pressure homogenizer for oil-in-water emulsions. *Chem. Eng. Process. Process. Intensif.* 160, 108249.
- Parthasarathy, S., Ying, T.Siah, Manickam, S., 2013. Generation and optimization of palm oil-based oil-in-water (O/W) submicron-emulsions and encapsulation of curcumin using a liquid whistle hydrodynamic cavitation reactor (LWHCRC). *Ind. Eng. Chem. Res.* 52 (34), 11829–11837.
- Patil, L., Gogate, P.R., 2018. Large scale emulsification of turmeric oil in skimmed milk using different cavitation reactors: a comparative analysis. *Chem. Eng. Process. Process. Intensif.* 126, 90–99.
- Pawar, S.K., et al., 2017. Sonochemical effect induced by hydrodynamic cavitation: Comparison of venturi/orifice flow geometries. *AIChE J.* 63 (10), 4705–4716.
- Perrier-Cornet, J.M., Marie, P., Gervais, P., 2005. Comparison of emulsification efficiency of protein-stabilized oil-in-water emulsions using jet, high pressure and colloid mill homogenization. *J. Food Eng.* 66 (2), 211–217.
- Politova, N., Tcholakova, S., Denkov, N.D., 2017. Factors affecting the stability of water-oil-water emulsion films. *Colloids Surf. A Physicochem. Eng. Asp.* 522, 608–620.
- Qin, C., et al., 2016. CFD-PBM simulation of droplets size distribution in rotor-stator mixing devices. *Chem. Eng. Sci.* 155, 16–26.
- Raikar, N.B., et al., 2009. Applications of population balance equation modeling to pharmaceutical emulsions. 2009 IEEE 35th Annu. Northeast Bioeng. Conf.
- Ramisetty, K.A., Pandit, A.B., Gogate, P.R., 2014. Novel approach of producing oil in water emulsion using hydrodynamic cavitation reactor. *Ind. Eng. Chem. Res.* 53 (42), 16508–16515.
- Ranade, V.V., 2002. *Computational Flow Modeling for Chemical Reactor Engineering*. Academic Press. Vol. 5.
- Ranade, V.V., et al., 2022. *Hydrodynamic Cavitation: Devices, Design and Applications*. John Wiley & Sons.
- Ranade, V.V., 2022. Modeling of Hydrodynamic Cavitation Reactors: Reflections on Present Status and Path Forward. *ACS Eng. Au* 2 (6), 461–476.
- Ranade, N.V., Ranade, V.V., 2023. ANN based surrogate model for key Physico-chemical effects of cavitation. *Ultrason. Sonochem.* 94, 106327.
- Ranade, V.V., Utikar, R.P., 2022. *Multiphase Flows for Process Industries: Fundamentals and Applications*. John Wiley & Sons.
- Sarvothaman, V.P., et al., 2024. Evaluating performance of vortex-diode based hydrodynamic cavitation device scale and pressure drop using coumarin dosimetry. *Chem. Eng. J.* 481, 148593.
- Sarvothaman, V.P., Simpson, A.T., Ranade, V.V., 2019. Modelling of vortex based hydrodynamic cavitation reactors. *Chem. Eng. J.* 377, 119639.
- Schlender, M., Spengler, A., Schuchmann, H.P., 2015. High-pressure emulsion formation in cylindrical coaxial orifices: Influence of cavitation induced pattern on oil drop size. *Int. J. Multiph. Flow.* 74, 84–95.
- Shamami, K., Birouk, M., 2008. Assessment of the performances of RANS models for simulating swirling flows in a can-combustor. *Open Aerosp. Eng. J.* 1, 8–27.
- Simpson, A., Ranade, V.V., 2019b. 110th Anniversary: Comparison of Cavitation Devices Based on Linear and Swirling Flows: Hydrodynamic Characteristics. *Ind. Eng. Chem. Res.* 58 (31), 14488–14509.
- Simpson, A., Ranade, V.V., 2019a. Modeling hydrodynamic cavitation in venturi: influence of venturi configuration on inception and extent of cavitation. *AIChE J.* 65 (1), 421–433.
- Simpson, A., Ranade, V.V., 2019a. Flow characteristics of vortex based cavitation devices. *AIChE J.* 65 (9).
- Singhal, A., et al., 2002. Mathematical basis and validation of the full cavitation model. *J. Fluids ENG. Trans. ASME J. Fluid Eng.* 124.
- Sun, X., et al., 2021. Experimental and numerical studies on the cavitation in an advanced rotational hydrodynamic cavitation reactor for water treatment. *Ultrason. Sonochem.* 70, 105311.
- Thaker, A.H., Madane, K.R., Ranade, V.V., 2023. Influence of viscosity and device scale on pressure drop and cavitation inception: Vortex based cavitation devices. *Chem. Eng. J.* 474, 145943.
- Thaker, A.H., Ranade, V.V., 2022. Towards harnessing hydrodynamic cavitation for producing emulsions: breakage of an oil drop in a vortex based cavitation device. *Chem. Eng. Process. Process. Intensif.* 180.
- Thaker, A.H., Ranade, V.V., 2023a. Emulsions using a vortex-based cavitation device: influence of number of passes, pressure drop, and device scale on droplet size distributions. *Ind. Eng. Chem. Res.* 62 (45), 18837–18851.
- Thaker, A.H., Ranade, V.V., 2023b. Drop breakage in a single-pass through vortex-based cavitation device: experiments and modeling. *AIChE J.* 69 (1), e17512.
- Upadhyay, M., Ranade, V.V., 2025. Dense coconut oil-in-water (CO-water) emulsification via a vortex-based cavitation device. *Chem. Eng. Technol.* 48 (5), e70015.
- Upadhyay, M., Ravi, A., Ranade, V.V., 2024. Dense oil in water emulsions using vortex-based hydrodynamic cavitation: effective viscosity, sauter mean diameter, and droplet size distribution. *Ind. Eng. Chem. Res.* 63 (11), 4977–4990.
- Vivek Ranade, A.K., Vinay Bhandari, *Vortex diodes as effluent treatment devices*, W.I.P. Organization, Editor. 2013.
- Wang, Z., et al., 2025. Multiscale investigation of cavitation surge characteristics in the swirling flow using Eulerian–Lagrangian method. *Ultrason. Sonochem.* 120, 107466.
- Yang, F., et al., 2018. Swirling cavitation improves the emulsifying properties of commercial soy protein isolate. *Ultrason. Sonochem.* 42, 471–481.
- Ye, K., et al., 2022. Influence of fluid viscosity on cavitation characteristics of a helico-axial multiphase pump (HAMP). *Energies* 15. <https://doi.org/10.3390/en15218149>.
- Zhang, Z., et al., 2016. Hydrodynamic cavitation as an efficient method for the formation of sub-100 nm O/W emulsions with high stability. *Chin. J. Chem. Eng.* 24 (10), 1477–1480.